

Comparative Assessment of the Ligand and Metal Ion Binding Properties of Integrins $\alpha 9\beta 1$ and $\alpha 4\beta 1$

R. Blake Pepinsky,^{*,‡} Richard A. Mumford,[§] Ling Ling Chen,[‡] Diane Leone,[‡] Suzanne E. Amo,[§] Gail Van Riper,[§] Adrian Whitty,[‡] Brian Dolinski,[‡] Roy R. Lobb,[‡] Dennis C. Dean,[§] Linda L. Chang,[§] Conrad E. Raab,[§] Qian Si,[§] William K. Hagmann,[§] and Russell B. Lingham^{*,§}

Biogen, Inc., 14 Cambridge Center, Cambridge, Massachusetts 02142, and Merck and Company, Inc., 126 East Lincoln Avenue, Rahway, New Jersey 07065

Received January 9, 2002; Revised Manuscript Received April 9, 2002

ABSTRACT: Integrins $\alpha 9\beta 1$ and $\alpha 4\beta 1$ form a distinct structural class, but while $\alpha 4\beta 1$ has been subjected to extensive study, $\alpha 9\beta 1$ remains poorly characterized. We have used the small molecule *N*-(benzenesulfonyl)-(L)-prolyl-(L)-*O*-(1-pyrrolidinylcarbonyl)tyrosine (**3**) to investigate the biochemical properties of $\alpha 9\beta 1$ and directly compare these properties with those of $\alpha 4\beta 1$. Compound **3** has a high affinity for both integrins with K_D values of ≤ 3 and 180 pM for $\alpha 9\beta 1$ in 1 mM Mn^{2+} (activating) and 1 mM Ca^{2+} and 1 mM Mg^{2+} (nonactivating) conditions and ≤ 5 and 730 pM for $\alpha 4\beta 1$ under the corresponding conditions. Ca^{2+} treatment promoted the binding of **3** to both integrins ($EC_{50} = 30 \mu M$ Ca^{2+} in both cases). Compound **3** binding to both integrins was also stimulated by the addition of the activating monoclonal antibody TS2/16. These findings indicate that the mechanisms by which metal ions and TS2/16 regulate ligand binding to $\alpha 9\beta 1$ and $\alpha 4\beta 1$ are similar. The binding of **3** to both integrins induced the mAb 9EG7 LIBS epitope, a property consistent with occupancy of the receptor's ligand binding site by **3**. But whereas EGTA treatment inhibited the binding of 9EG7 to $\alpha 4\beta 1$, it stimulated the binding of 9EG7 to $\alpha 9\beta 1$. The 9EG7 and TS2/16 effects point to contributions of the $\beta 1$ -chains on binding. Cross-linking data revealed that the integrin α -chains are also involved in binding the small molecule, as stable linkages were observed on both the $\alpha 9$ chain of $\alpha 9\beta 1$ and the $\alpha 4$ chain of $\alpha 4\beta 1$. Extensive structure–activity analyses with natural and synthetic ligands indicate distinct features of the ligand binding pockets. Most notable was the estimated >1000 -fold difference in the affinity of the integrins for VCAM-1, which binds $\alpha 4\beta 1$ with an apparent K_D of 10 nM and $\alpha 9\beta 1$ with an apparent K_D of $>10 \mu M$. Differences were also seen in the binding of $\alpha 9\beta 1$ and $\alpha 4\beta 1$ to osteopontin. Compound **3** competed effectively for the binding of VCAM-1 and osteopontin to both integrins. While these studies show many similarities in the biochemical properties of $\alpha 9\beta 1$ and $\alpha 4\beta 1$, they identify important differences in their structure and function that can be exploited in the design of selective $\alpha 9\beta 1$ and $\alpha 4\beta 1$ inhibitors.

Integrins are a large family of cell surface receptors that mediate cell–cell and cell–matrix interactions and signal transduction (see refs 1 and 2 for reviews). They exist as noncovalent $\alpha\beta$ heterodimers of different combinations of the α - and β -chains and share extensive structural homology. Eighteen α -chains and eight β -chains have been identified. Integrin function is regulated by the relative affinity and availability of its ligands. Integrin–ligand interactions are typically of low affinity, and binding presumably results from multivalent interactions (3–8). Integrins undergo an activation step that increases their affinity for their ligand, which can be mimicked through the addition of the divalent cation Mn^{2+} , or certain specific antibodies (9–11). The mechanisms leading to activation are believed to occur, at least in part, through conformational changes of the integrin. Identifying biologically relevant ligand–integrin interactions has been

complicated since most integrins bind more than one ligand and most known ligands can support the binding of multiple integrins (see ref 12 for review). The regulation of integrin function by metal ions is complex and is not fully understood (12–17). Integrin α -subunits contain multiple Ca^{2+} binding loops (1, 18), which are in close proximity to ligand binding sites (19, 20). This region of the α -chain is made up of seven sequence repeats of about 60 amino acids each, which are organized in a β -propeller fold (19–21). The β -chain contains a second type of metal binding/ligand binding motif that shares homology with the A-domain of von Willebrand's factor (21–23). A homologous structure is present in some α -subunits as well (24–27). This A-domain structure, or I-domain as it is sometimes referred to, is inserted between repeats 2 and 3 of the β -propeller fold. Regulation of ligand binding by cations is further complicated by the fact that some metal binding sites have an inhibitory role (12, 14, 15) and that ligand affinity influences metal ion regulation (28).

The leukocyte integrin $\alpha 4\beta 1$ is an attractive therapeutic target and has been the subject of extensive evaluation. $\alpha 4\beta 1$

* To whom correspondence should be addressed. Telephone: (617) 679-3310 and (732) 594-6223. Fax: (617) 679-2616 and (732) 594-7422. E-mail: blake_pepinsky@biogen.com and russell_ingham@merck.com.

[‡] Biogen, Inc.

[§] Merck and Co., Inc.

regulates cell migration into tissues during inflammatory responses and normal lymphocyte trafficking (29–31) and provides a key costimulatory signal supporting cell activation (32–36). In vivo studies using blocking monoclonal antibodies (30) and inhibitory peptides (37–39) have demonstrated a critical role for $\alpha 4$ integrins in leukocyte-mediated inflammation. Recent positive phase II data using the anti- $\alpha 4$ antibody Antegren in patients with multiple sclerosis have validated $\alpha 4\beta 1$ as an important clinical target (40). $\alpha 4\beta 1$ mediates cell adhesion by binding to either of two protein ligands, vascular cell adhesion molecule-1 (VCAM-1)¹ or the alternatively spliced connecting segment 1- (CS1-) containing fibronectin variant (41–44). More recently, other potential ligands have been identified (45, 46); however, the biological significance of these interactions is less clear. The key residues in VCAM-1 (QIDSP) and CS1 (EILDVP) necessary for their interactions with $\alpha 4\beta 1$ have been defined by molecular and biochemical techniques (3, 47). Many groups have used these sequences as starting points to develop small molecule inhibitors that can block the interaction between $\alpha 4\beta 1$ and its ligands (48–52).

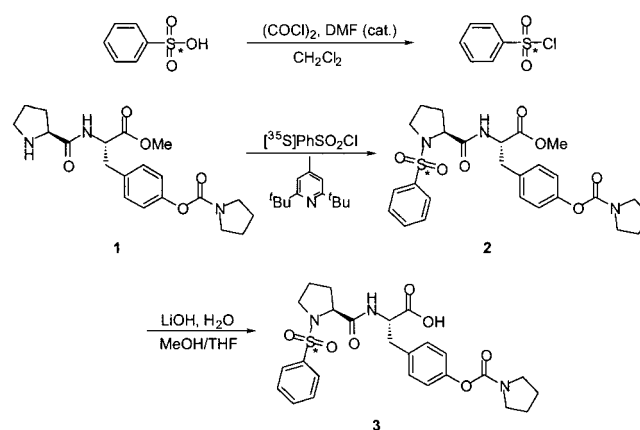
Structurally, the integrin $\alpha 9$ chain is closely related to the $\alpha 4$ chain. On the basis of sequence homology, $\alpha 9$ and $\alpha 4$ are the only known integrin α -chains that lack both an inserted A-domain and an extracellular disulfide-linked cleavage site (53). Further similarities are found in the functional properties of $\alpha 4\beta 1$ and $\alpha 9\beta 1$ as both integrins bind osteopontin and VCAM-1 (46, 54, 55) and both integrins utilize the same signal transduction pathways (56). The most notable difference between $\alpha 4\beta 1$ and $\alpha 9\beta 1$ is in their cellular distribution. While $\alpha 4\beta 1$ expression is limited largely to leukocytes, $\alpha 9\beta 1$ is widely expressed in epithelia, in smooth and skeletal muscle, and on neutrophils (53, 55, 57). Studies of $\alpha 9$ (–/–) knock-out mice revealed that the animals were normal at birth but developed respiratory failure and died at age 6–12 days, suggesting an involvement of the integrin in the normal development of the lymphatic system (58).

Previously, we used two radiolabeled $\alpha 4\beta 1$ inhibitors, BIO1211 (16) and BIO7662 (28), as probes for evaluating the biochemical properties of $\alpha 4\beta 1$. These studies revealed novel features about mechanisms regulating the affinity of the integrin for ligand and metal ion binding. In studying

the selectivity of different classes of $\alpha 4\beta 1$ inhibitors, we identified several small molecule inhibitor series that also inhibited $\alpha 4\beta 7$ and $\alpha 9\beta 1$ function, two integrins that share many of the same ligands as $\alpha 4\beta 1$. One inhibitor in particular, *N*-(benzenesulfonyl)-(L)-prolyl-(L)-O-(1-pyrrolidinylcarbonyl)tyrosine (**3**), was of special interest because of its high affinity for $\alpha 9\beta 1$, thus providing a unique opportunity to study the biochemical properties of this less characterized integrin. Here, we compare and contrast the biochemical properties of $\alpha 9\beta 1$ and $\alpha 4\beta 1$, using [³⁵S]-sulfonyl-labeled **3** as a probe for function. These studies provide the first detailed analysis of the ligand and metal ion binding properties of $\alpha 9\beta 1$ and a direct comparison of these properties with those of $\alpha 4\beta 1$.

EXPERIMENTAL PROCEDURES

*Synthesis of [³⁵S]-N-(Benzenesulfonyl)-(L)-prolyl-(L)-O-(1-pyrrolidinylcarbonyl)tyrosine (**3**).*



[³⁵S]Benzenesulfonyl Chloride. A solution of [³⁵S]benzenesulfonic acid in ethanol (110 mCi, specific activity = 1435 Ci/mmol, obtained commercially from Perkin-Elmer Life Sciences) was transferred to a 20 mL screw-cap vial. The solvent was evaporated in a stream of N₂ at 65 °C, and the residue was dissolved in anhydrous CH₂Cl₂ (6 mL). Oxalyl chloride (250 μ L) and anhydrous dimethylformamide (1 drop) were added with evolution of gas, and the reaction was stirred at room temperature. After 1 h, the radioactive content of the solution was determined by liquid scintillation counting to be 101 mCi. The solution was cooled to 0 °C, water (3 mL) added, and the mixture stirred for 10 min before being warmed to room temperature and stirred for 30 min. The solution was then washed quickly with 5% aqueous NaHCO₃ (2 \times 2 mL) and 1% aqueous NaHSO₃ (1 \times 2 mL). The combined aqueous layers were counted (11 mCi). The organic layer was dried over Na₂SO₄ and filtered twice, at which point liquid scintillation counting showed that the solution contained 89 mCi (81%). The material was analyzed by HPLC (99.0% radiochemical purity, Phenomenex Polar RP, 4.6 \times 250 mm, 210/254 nm, 1.0 mL/min, 50% acetonitrile–0.1% aqueous HClO₄ isocratic for 20 min; *t_r* for [³⁵S]benzenesulfonic acid = 2.7 min, *t_r* for [³⁵S]-benzenesulfonyl chloride = 12.8 min) and used without purification in subsequent reactions.

[³⁵S]-N-(Benzenesulfonyl)-(L)-prolyl-(L)-O-(1-pyrrolidinylcarbonyl)tyrosine Methyl Ester (2**).** A solution of [³⁵S]-benzenesulfonyl chloride (24 mCi) in CH₂Cl₂ was concen-

¹ Abbreviations: **3**, *N*-(benzenesulfonyl)-(L)-prolyl-(L)-O-(1-pyrrolidinylcarbonyl)tyrosine; mAb, monoclonal antibody; LIBS, ligand-induced binding site; VCAM-1, vascular cell adhesion molecule-1; CS1, connecting segment 1; BIO1211, 4-[*N'*-(2-methylphenyl)ureido]phenylacetyl-leucine-aspartic acid-valine-proline; BIO7662, 2(*S*)-[(1-benzenesulfonylpyrrolidine-2(*S*)-carbonyl)amino]-4-[4-methyl-2(*S*)-(methyl-2-[4-(3-*o*-tolylureido)phenyl]acetyl)amino]pentanoylamino]butyric acid; HPLC, high-pressure liquid chromatography; TFA, trifluoroacetic acid; SDS–PAGE, sodium dodecyl sulfate–polyacrylamide gel electrophoresis; BSA, bovine serum albumin; PBS, phosphate-buffered saline; TBS, Tris-buffered saline; Hepes, *N*-(2-hydroxyethyl)piperazine-*N'*-2-ethanesulfonic acid; Tris, 2-amino-2-(hydroxymethyl)-1,3-propanediol; EDTA, ethylenediaminetetraacetic acid; EGTA, ethylene glycol bis-(β -aminoethyl ether)-*N,N,N',N'*-tetraacetic acid; FACS, fluorescence-activated cell sorter; PMNs, peripheral mononuclear cells; OPN, osteopontin; SAR, structure–activity relationship; MIDAS, metal ion-dependent adhesion site; BIO1494, 4-[*N'*-(2-methylphenyl)ureido]phenylacetyl-(ϵ -aminoethyl)lysine-aspartic acid-valine-proline; **4a**, (4*R*)-4-[(4-azido-2-hydroxybenzoyl)amino]-1-(phenylsulfonyl)-L-prolyl-O-(pyrrolidin-1-ylcarbonyl)-L-tyrosine; **4b**, 1-[[3-({6-[(4-azido-2-hydroxybenzoyl)amino]hexanoyl)amino}phenyl)sulfonyl]-L-prolyl-O-(pyrrolidin-1-ylcarbonyl)-L-tyrosine.

trated to $\sim 150 \mu\text{L}$ at atmospheric pressure in a short-path distillation apparatus. This was added to a solution of amine **1** (10.5 mg) and 2,6-di-*tert*-butyl-4-methylpyridine (6.0 mg) in anhydrous CH_2Cl_2 (50 μL), rinsing the distillation flask out with further anhydrous CH_2Cl_2 (200 μL). The reaction mixture was stirred at room temperature for 3 h, at which time HPLC analysis showed 98% sulfonamide ester **2** formation (same HPLC method as above; t_r for **1** = 4.6 min, t_r for [^{35}S]benzenesulfonyl chloride = 12.8 min; t_r for **2** = 13.9 min). The reaction was then diluted with ethyl acetate (5 mL) and 1 N aqueous HCl (5 mL). The layers were separated, and the aqueous layer was extracted with ethyl acetate ($3 \times 10 \text{ mL}$). The combined organics were washed with H_2O ($1 \times 10 \text{ mL}$), then dried over Na_2SO_4 , filtered, and concentrated in vacuo. The residue was taken up in methanol (10 mL), radioactivity was quantified by liquid scintillation counting (24 mCi), and the residue was analyzed by HPLC (>99% radiochemical purity, same HPLC method as above). The material was used in the next step without purification. The identity of the compound was confirmed by coelution with an authentic sample of unlabeled **2**.

[^{35}S]-*N*-(Benzenesulfonyl)-(L)-prolyl-(L)-O-(1-pyrrolidinyl-carbonyl)tyrosine (**3**). The methanolic solution of [^{35}S]-sulfonamide ester **2** was concentrated in vacuo, and the residue was taken up in 1:1 methanol/tetrahydrofuran (1 mL) and cooled to 0 °C. A solution of $\text{LiOH}\cdot\text{H}_2\text{O}$ (12 mg) in water (0.5 mL) was added dropwise over 20 min, and the reaction mixture was stirred for a further 20 min at 0 °C. HPLC analysis at this stage showed complete saponification of **2** (same HPLC method as above; t_r for **3** = 8.5 min, t_r for **2** = 13.9 min). The reaction mixture was acidified with 1 N HCl and then diluted with water (5 mL) and ethyl acetate (5 mL). The layers were separated, and the aqueous layer was extracted with ethyl acetate ($4 \times 10 \text{ mL}$). The combined organics were dried over Na_2SO_4 , filtered, and concentrated in vacuo. The residue was taken up in acetonitrile and counted (21 mCi). The material was purified twice by semipreparative HPLC (Zorbax RX-C8 column, $10 \times 250 \text{ mm}$, 210 nm, 5.0 mL/min, 35% acetonitrile–0.1% aqueous TFA isocratic for 30 min; t_r for **3** = 24 min), each time collecting the compound as a single fraction ($\sim 10 \text{ mL}$), diluting it with water (30 mL), and passing the solution through a C_{18} Sep-Pak. After the Sep-Pak was washed with water, the product was eluted with methanol. After the second purification, the methanol solution of **3** was counted (16.5 mCi) and analyzed by HPLC (99.5% radiochemical purity, Zorbax RX-C₈, $4.6 \times 250 \text{ mm}$, 210/254 nm, 1.0 mL/min, 40% acetonitrile–0.1% aqueous TFA isocratic for 20 min; t_r for [^{35}S]sulfonamide = 15.2 min). The solution of [^{35}S]-**3** (16.5 mCi) in 4.5 mL of methanol was degassed (N_2 bubbling) and stored at –30 °C. The identity of the compound was confirmed by coelution with an authentic sample of unlabeled **3**. The specific activity was determined to be 1172 Ci/mmol by liquid chromatography/mass spectrometry.

*Binding of [^{35}S]-**3** to $\alpha 9\beta 1$ Expressing Cells.* Jurkat and K562 cells (from the American Type Culture Collection, Rockville, MD), $\alpha 1$ -transfected K562 cells (Beth Browning, Biogen, Inc.), $\alpha 9$ -transfected K562 cells (Diane Leone, Biogen, Inc.), $\alpha 6$ -transfected K562 cells (a gift of A. Sonnenberg, The Netherlands Cancer Institute, Amsterdam, The Netherlands), and $\alpha 2$ - and $\alpha 4$ -transfected K562 cells

(gifts from M. Hemler, Dana Farber Cancer Institute, Boston, MA) were maintained in RPMI-1640 medium plus 10% fetal bovine serum at 37 °C in a tissue culture incubator. Cells were periodically monitored for high-level surface expression of the appropriate integrin by FACS analysis. For binding studies, the cells were pelleted by centrifugation, washed two times with TBS [50 mM Tris-HCl, 150 mM NaCl, 0.1% bovine serum albumin (BSA), 2 mM glucose, 10 mM Hepes, pH 7.4], suspended at approximately 2×10^6 cells/mL in TBS, and counted using a Neubauer hemocytometer. The cells were further diluted with TBS to the concentration indicated and treated with [^{35}S]-**3** at room temperature. The cells were then pelleted by centrifugation, resuspended in 100 μL of TBS plus Mn^{2+} , and transferred to a scintillation vial containing 2.9 mL of ScintiVerse II (Fisher). Cell-associated radioactivity was quantified by scintillation counting. All studies were performed in siliconized 1.5 mL Eppendorf tubes with a standard 1 mL sample volume. Binding studies unless indicated were performed in TBS plus 1 mM MnCl_2 , 1 mM CaCl_2 plus 1 mM MgCl_2 , or 1 mM CaCl_2 as described. Rate constants for dissociation were generally derived from a single-exponential curve fit. However, where indicated, a double-exponential fit was used to account for an initial burst of dissociation accounting for $\leq 15\%$ of bound counts. In these cases, the reported k_{off} values are based on the slow phase of dissociation that accounted for $\geq 85\%$ of bound counts.

In selected studies binding was performed on freshly isolated human PMNs and on human melanoma G-361 cells (46). Binding was performed in the presence of 100 nM BIO5192, a specific inhibitor of $\alpha 4\beta 1$ (28), to block any potential association of **3** with $\alpha 4\beta 1$ present on G-361 cells and human neutrophils. G-361 human epithelial melanoma cells (CRL-1424 from the American Type Culture Collection, Rockville, MD) were maintained in a tissue culture incubator at 37 °C in McCoy's medium supplemented with 10% fetal bovine serum, 100 units/mL penicillin, 100 $\mu\text{g}/\text{mL}$ streptomycin, and 2 mM L-glutamine. Cells were removed from flasks with Versene solution (Gibco-BRL, 1:5000 dilution). For receptor binding studies, the harvested cells were pelleted by centrifugation, washed twice with Ca^{2+} , Mg^{2+} -free phosphate-buffered saline (PBS), and suspended in PBS at a concentration of $5 \times 10^6/\text{mL}$ in binding buffer (25 mM Hepes, 150 mM NaCl, 0.1% bovine serum albumin, 3 mM KCl, pH 7.4, 2 mM glucose). G-361 cells were resuspended without cations and preincubated with 100 nM BIO5192 for 15 min at room temperature. Receptor binding assays were performed in Millipore Unifilter plates (MHVB4550) in binding buffer containing either 1 mM Ca^{2+} and Mg^{2+} or 1 mM Mn^{2+} . Dilutions of inhibitors were prepared in dimethyl sulfoxide at 100 times the desired concentration. G-361 cells at a final concentration of 1×10^5 cells/well were added to wells containing 200 pM [^{35}S]-**3**, binding buffer, and 1 μL of test compound. The plates were incubated at 37 °C for 60 min. The assay suspension was filtered using a vacuum apparatus, and the plates were washed two times with 100 μL of cold binding buffer containing the appropriate cations. The filters were dried at room temperature, and 200 μL of MicroScint-20 was added to the wells. Radioactive counts were quantified in a Packard TopCount.

Integrin levels of the G-361 cell line were determined by fluorescence-assisted cell sorter (FACS) analysis. G-361 cells

were harvested as described above and used at 1×10^6 /tube in 5% fetal calf serum in PBS. Nonspecific binding on cells was blocked with 100 $\mu\text{g/mL}$ goat IgG (Jackson Laboratories) at room temperature for 15 min. Cells were then incubated with primary antibodies (1–5 $\mu\text{g/mL}$) for 30 min at room temperature, using integrin chain-specific mAbs P4G11 (β 1), FB12 (α 1), P1E6 (α 2), P1B5 (α 3), P1D6 (α 5), and Y9A2 (α 9), which were obtained from Chemicon, and mAb HP2/1 (α 4), which was from Beckman Coulter. Cells were pelleted by centrifugation and washed twice with 3 mL of 5% fetal calf serum in PBS. Secondary anti-mouse antibody conjugated to fluorescein isothiocyanate (FITC) was added to cells, and the incubation was continued for 30 min at room temperature. Cells were washed as above and resuspended in 300 μL of propidium iodide, and fluorescence was quantified with a FACScan flow cytometer (Becton Dickinson and Co.). Integrin levels/cell were calculated from FACS data using a Quantitative MESF (Molecules of Equivalent Soluble Fluorochromes) FITC bead kit from Bangs Laboratories, Inc. (Fishers, IN) following the manufacturer's recommended protocol. Expression levels for the following integrins were obtained: α 4, 4400 receptors/cell; α 9, 17000 receptors/cell; β 1, 25000 receptors/cell; α 1, 5300 receptors/cell; α 2, 8900 receptors/cell; α 3, 1400 receptors/cell; and α 5, 490 receptors/cell.

For preparation of neutrophils, venous blood from healthy adult volunteers was collected into 50 mL polypropylene syringes containing 20 units/mL heparin. Blood was transferred to 50 mL polypropylene centrifuge tubes, and granulocytes were isolated with modifications of the procedure as described (59). Blood was centrifuged (1300g, no brake) for 15 min at room temperature, and the platelet-rich plasma was removed and discarded. The remaining cells were reconstituted to the original blood volume with 145 mM NaCl. Three milliliters of 3% dextran was added for every 10 mL of original blood volume and allowed to sediment for 60–90 min at room temperature. The upper layer was removed to a 50 mL Falcon tube, and 1 mL of cold Histopaque (Ficoll, density 1.077 g/mL) per every 4 mL of upper layer was added to the bottom of the tube and centrifuged (1300g, no brake) at 4 °C for 20 min. The supernatant fluid was discarded, and the pellet was suspended in PBS and centrifuged (1300g, no brake) for 5 min. Red blood cells remaining in the pellet were lysed in 10 mL of ACK lysing buffer (Gibco-BRL) for 5 min, diluted with PBS, and centrifuged as above. The pellet was washed and suspended in PBS and counted using a Neubauer hemocytometer. Receptor binding studies were carried out as described above for the G-361 cells; however, in addition to preincubation with BIO5192, neutrophils were activated with phorbol myristate acetate (50 ng/mL). The final cell concentration was 1×10^6 neutrophils per assay.

Selectivity Studies with Alternative Integrins. The selectivity of **3** to other integrins was studied in adhesion assays using cells expressing specific integrins with their respective immobilized ligands. The ligands were immobilized in microtiter wells at 4 °C overnight at the indicated concentrations. Cells (4.0×10^6 /mL), labeled with 2',7'-bis(carboxyethyl)-5(6)-carboxyfluorescein acetomethyl ester, were incubated in ligand-coated wells for 30 min at room temperature, unless otherwise noted, with inhibitor, or vehicle, in the

presence of 1 mM MnCl_2 . After being washed, bound cells were quantified by fluorescence at 530 nm. For each integrin assay an appropriate inhibitor was included as positive control. The ligands used for measuring adhesion of each integrin were as follows: α 1 β 1, human placental type IV collagen (0.5 $\mu\text{g/mL}$), α 1-K562 cells, assay run at 37 °C; α 2 β 1, rat tail collagen I (5 $\mu\text{g/mL}$), α 2-K562 cells, assay run at 37 °C; α 5 β 1, human 120 kDa fibronectin fragment (5 $\mu\text{g/mL}$), K562 cells. For α 4 β 7, plates were coated with 1 $\mu\text{g/mL}$ BSA–N-[4-(6-aminohexane-1-sulfonylamino)-2,6-dichlorobenzoyl]-4-(2,6-dimethoxyphenyl)-L-phenylalanine trifluoroacetate conjugate that was generated by reacting BSA–maleimide (Pierce) with the 2-iminothiolane derivative of N-[4-(6-aminohexane-1-sulfonylamino)-2,6-dichlorobenzoyl]-4-(2,6-dimethoxyphenyl)-L-phenylalanine at a molar ratio of 1:10. JY cells were used to assess binding. The binding of **3** to α 4 β 7 was evaluated in 1 mM Mn^{2+} and in 1 mM Ca^{2+} and 1 mM Mg^{2+} . Binding of **3** to α IIb β 3 was evaluated in a platelet aggregation assay. Human citrated platelet-rich plasma was diluted to 2.0×10^8 platelets/mL with platelet-poor plasma and aggregated with 20 μM ADP with monitoring in an aggregometer.

Purification of α 9 β 1. An enriched population of the α 9-K562 cells that exhibited high levels of α 9 expression, on average 100000 copies per cell, was obtained by FACS sorting, and this subclone was used for all subsequent work. The cells were grown at 37 °C in a 10 L bioreactor in RPMI-1640 medium supplemented with 10% fetal bovine serum, 1 mg/mL G418, 10 $\mu\text{g/mL}$ gentamicin sulfate, and 50 $\mu\text{g/mL}$ streptomycin. Cells were collected by centrifugation and lysed in 1% Nonidet P40, 25 mM Tris-HCl, pH 7.4, 1 mM CaCl_2 , 1 mM MgCl_2 , 1 mM MnCl_2 , 2% BSA, and 1 mM phenylmethanesulfonyl fluoride at 1×10^8 cells/mL of lysis buffer. The lysates were clarified by centrifugation and stored at –70 °C for subsequent use. Fifteen milliliters of the α 9-K562 cell lysate was incubated for 2 h at 4 °C with 0.5 mL of mAb-13–Sepharose 4B that had been conjugated with antibody at 5 mg/mL resin. The resin was collected in a column and washed with two column volumes of lysis buffer without BSA and then with 10 volumes of 0.1% Triton X-100, 25 mM Tris-HCl, pH 7.4, 1 mM CaCl_2 , and 1 mM MgCl_2 . α 9 β 1 was eluted with 10 mM sodium acetate, pH 3.2, 0.1% Triton X-100, 1 mM CaCl_2 , and 1 mM MgCl_2 and immediately neutralized with Hepes buffer, pH 8.0. Fractions were assayed for α 9 β 1 in a sandwich ELISA and for total protein using the BCA microprotein assay from Pierce. Peak fractions were pooled, aliquoted, and stored at –70 °C. The mAb-13 (60) was purified from mouse ascites on protein A–Sepharose (Amersham Pharmacia Biotech). Integrin α 4 β 1 was purified as previously described (61).

Synthesis of (4R)-4-[(4-Azido-2-hydroxybenzoyl)amino]-1-(phenylsulfonyl)-L-prolyl-O-(pyrrolidin-1-ylcarbonyl)-L-tyrosine (4a) and 1-[[3-[(6-[(4-Azido-2-hydroxybenzoyl)amino]hexanoyl)amino]phenyl]sulfonyl]-L-prolyl-O-(pyrrolidin-1-ylcarbonyl)-L-tyrosine (4b). For cross-linking studies, two derivatives of **3** were synthesized that contained the photoreactive cross-linker azidosalicylic acid: one with the azido function attached to the proline ring (**4a**) and the other with the azido attached to the benzenesulfonyl moiety (**4b**). Compounds **4a** and **4b** were selected from a more extensive set of derivatives that was synthesized because the

modifications had not significantly altered their affinity for $\alpha 4\beta 1$. Compounds **4a** and **4b** were monoiodinated on the azidosalicylic acid moiety using the chloramine T method.

Synthesis of 4a. Triphosgen (1.1 mmol) and Fmoc-Tyr-*O*-*tert*-butyl (3 mmol) were placed in an oven-dried round-bottomed flask. Anhydrous CH_2Cl_2 (20 mL) was added, and then *N,N*-diisopropylethylamine (3 mmol) was added dropwise with a syringe. The mixture was stirred under nitrogen for 30 min at room temperature and then for 2 h at 80 °C. HPLC analysis indicated complete conversion of the Fmoc-Tyr-*O*-*tert*-butyl to Fmoc-Tyr-*O*-methyl chloroformate. The mixture was chilled to -15 °C under nitrogen, and 3 mmol of pyrrolidine (dissolved in 10 mL CH_2Cl_2) was added with a syringe. The reaction was stirred for 1 h at -15 °C and another 1 h at room temperature. CH_2Cl_2 (30 mL) was added to the flask, and the reaction mixture was extracted three times each with 1 N HCl and with saturated NaHCO_3 and one time with supersaturated NaCl. The CH_2Cl_2 layer was dried with MgSO_4 and concentrated in vacuo. The residue was dissolved in 3 mL of dimethylformamide. Two equivalents of 1,8-diazabicyclo[5.4.0]undec-7-ene was added, and the sample was stirred for 3 h. The resulting mixture was fractionated on a silica gel column in 5% methanol/95% CH_2Cl_2 to obtain 613 mg of pure NH_2 -Tyr(*O*-pyrrolidine carbamate)-*O*-methyl (70% yield). One millimole of (2*S*,4*R*)-Fmoc-4-amino-1-Boc-pyrrolidine-2-carboxylic acid (4-amino-proline) in 10 mL of CH_2Cl_2 was mixed with 1.1 mmol of the tyrosine carbamate methyl ester. The mixture was chilled to 0 °C, and 1.1 mmol of PyBOP and 2.2 mmol of *N,N*-diisopropylethylamine were added. After 3 h at room temperature with stirring, the reaction mixture was purified on a silica gel column (2% methanol/98% CH_2Cl_2) to obtain 364 mg of Fmoc-4-amino-Pro-Tyr(pyrrolidine carbamate)-*O*-methyl (90% yield). The Boc-protected Fmoc-4-amino-Pro-Tyr(pyrrolidine carbamate)-*O*-methyl was dissolved in CH_2Cl_2 and treated with gaseous HCl at 0 °C for 30 min. The solvent was evaporated to dryness, and the residue was used without further purification. The HCl-treated material (0.5 mmol) was dissolved in 5 mL of CH_2Cl_2 . Benzene-sulfonyl chloride (0.5 mmol) was added to the solution, which was chilled to 0 °C under nitrogen. *N,N*-Diisopropylethylamine (1.5 mmol) was added, and the mixture was stirred for 3 h. CH_2Cl_2 (20 mL) was added, and the reaction mixture was extracted three times with 1 N HCl. The organic layers were combined and washed with 1 N HCl (once), saturated NaHCO_3 (three times), and supersaturated NaCl (once). The Fmoc-protected material [0.2 mmol (crude weight)] in 2 mL of acetonitrile/water (70%/30%) was reacted with 2 equiv of 1,8-diazabicyclo[5.4.0]undec-7-ene for 2 h to remove the Fmoc. The mixture was HPLC purified. The pure, deprotected methyl ester (65 mg) was recovered (59% yield). The ester [50 mg (0.09 mmol)] was treated with 2 equiv of LiOH in 2 mL of tetrahydrofuran/water (50%/50%) overnight. The tetrahydrofuran was evaporated, and the residue was dissolved in 2 mL of acetonitrile/water (50%/50%). The resulting (4*R*)-4-ammonio-1-(phenylsulfonyl)-L-prolyl-*O*-(pyrrolidin-1-ylcarbonyl)-L-tyrosine trifluoroacetate derivative was HPLC purified. Ion spray mass spectrum: 530.6 Da (theoretical), 531.4 Da [$\text{M} + \text{H}$] (observed). (4*R*)-4-Ammonio-1-(phenylsulfonyl)-L-prolyl-*O*-(pyrrolidin-1-ylcarbonyl)-L-tyrosine trifluoroacetate [50 mg (0.094 mmol)]

in 0.5 mL of dimethylformamide was mixed with 0.2 mmol of *N,N*-diisopropylethylamine and 0.1 mmol of 4-azidosalicylic acid hydroxy succinimide ester for 3 h with stirring. The solvent was evaporated, and the residue was HPLC-purified to recover 27 mg of compound **4a** (40% yield). Ion spray mass spectrum of **4a**: 691.7 Da (theoretical), 692.2 Da [$\text{M} + \text{H}$] (observed).

Synthesis of 4b. Boc-Pro-OH (1 mmol) and 1 mmol of NH_2 -Tyr(pyrrolidine carbamate)-*O*-methyl were dissolved in 10 mL of CH_2Cl_2 at 0 °C. Benzotriazol-1-yloxytris(pyrrolidino)phosphonium hexafluorophosphate (1.2 mmol) was added to the cold solution followed by 2 mmol of *N,N*-diisopropylethylamine. The mixture was stirred for 3 h. CH_2Cl_2 (30 mL) was added, and the mixture was extracted with 1 N HCl (three times) and supersaturated NaCl (once). The solvent was evaporated, and the residue was silica gel column-purified (5% methanol/95% CH_2Cl_2) to obtain 415 mg of the product (85% yield). The Boc-protected dipeptide (0.5 mmol) in 5 mL of CH_2Cl_2 was treated at 0 °C for 30 min with gaseous HCl. The solvent was evaporated, and the residue was dissolved in CH_2Cl_2 . The solution was chilled to 0 °C under nitrogen, and 0.5 mmol of 3-nitrobenzenesulfonyl chloride was added followed by 1 mmol of *N,N*-diisopropylethylamine. The mixture was stirred for 1 h. CH_2Cl_2 (30 mL) was added to the mixture, and it was extracted with 1 N HCl (three times) and supersaturated NaCl (once) and freeze-dried. The dried nitro compound was dissolved in 5 mL of ethyl acetate containing 300 mg of 10% palladium/carbon. The mixture was stirred under hydrogen overnight. The mixture was filtered with Celite, and the solvent was evaporated. The 3-aminobenzenesulfonyl analogue was used for the next step without further purification. Boc-LC-OH (0.6 mmol) and 0.65 mmol of *N*-methylmorpholine were mixed in 5 mL of anhydrous CH_2Cl_2 . The mixture was cooled to -15 °C under nitrogen. After 5 min with stirring, 0.65 mmol of isobutyl chloroformate was introduced with a syringe. The mixture was stirred for 1 h at -15 °C and then for 1 h at room temperature. In a separate vessel, 0.5 mmol of the amino compound in 5 mL of anhydrous CH_2Cl_2 was treated with 2 equiv of NaH and heated to 60 °C under refluxing condenser. To the solution was added the Boc-LC chloroformate, and the mixture was stirred overnight at 85 °C under nitrogen. CH_2Cl_2 (15 mL) and 10 mL of 1 N HCl were added to the reaction mixture. The layers were separated, and the aqueous layer was extracted with CH_2Cl_2 (twice). The CH_2Cl_2 extracts were combined and washed with 1 N HCl (twice), saturated NaHCO_3 (twice), and supersaturated NaCl (once). The CH_2Cl_2 was evaporated down to 10 mL, and gaseous HCl was bubbled into the solution at 0 °C for 30 min to remove the Boc. The solvent was evaporated, and the residue was dissolved in 5 mL of water/tetrahydrofuran. Two equivalents of LiOH was added, and the sample was allowed to stir overnight. The tetrahydrofuran was evaporated, and 5 mL of acetonitrile was added to the residue. (Aminohexanoyl)-(3-aminobenzenesulfonyl)-Pro-Tyr(*O*-pyrrolidine carbamate)-OH was HPLC-purified from the mixture. The peptide [0.07 mmol (48 mg)] and 0.2 mmol of *N,N*-diisopropylethylamine were mixed with 0.07 mmol of 4-azidosalicyl-*O*-hydroxysuccinimidyl ester in 0.5 mL of dimethylformamide. The reaction was stirred for 3 h, and the solvent was evaporated.

Table 1: Integrin Selectivity Data for Compound **3**^a

activation state	K_D (nM)		IC_{50} (nM)				
	$\alpha 4\beta 1$	$\alpha 9\beta 1$	$\alpha 4\beta 7$	$\alpha 1\beta 1$	$\alpha 2\beta 1$	$\alpha 5\beta 1$	$\alpha IIB\beta 3$
1 mM Mn^{2+}	<0.005	<0.003	10 ^b	10000	22	76	>100000
1 mM Ca^{2+} and Mg^{2+}	0.73	0.18	400				

^a The selectivity of **3** toward the seven integrins indicated was tested in adhesion formats for $\alpha 4\beta 7$, $\alpha 1\beta 1$, $\alpha 2\beta 1$, and $\alpha 5\beta 1$, by platelet aggregation for $\alpha IIB\beta 3$, and by direct binding for $\alpha 4\beta 1$ and $\alpha 9\beta 1$ as described in Experimental Procedures. For adhesion assays, cell binding to 96-well plates coated with type IV collagen for $\alpha 1\beta 1$, collagen I for $\alpha 2\beta 1$, the 120 kDa fibronectin fragment for $\alpha 5\beta 1$, and a small molecule inhibitor-BSA conjugate for $\alpha 4\beta 7$ was assessed in the presence of serial dilutions of compound **3** (from 1 nM to 100 μ M). IC_{50} values were calculated from the concentration dependence of the inhibition curves. K_D values for the binding of [³⁵S]-**3** to $\alpha 4\beta 1$ and $\alpha 9\beta 1$ were calculated from kinetic measurements.

^b An IC_{50} value of 2.8 nM was determined by direct binding in a competition format using [¹²⁵I]VCAM-Ig as the probe (see below).

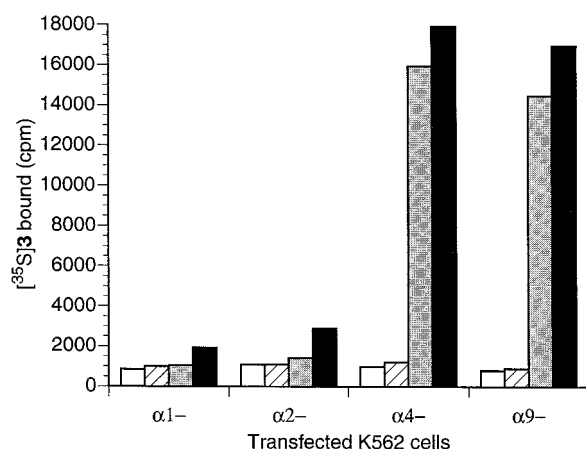


FIGURE 1: Specificity of [³⁵S]-**3** binding. [³⁵S]-**3** binding specificity was tested on K562 cells transfected with either the $\alpha 9$, $\alpha 4$, $\alpha 2$, or $\alpha 1$ gene (1×10^6 cells/mL). Cells were treated with 5 nM [³⁵S]-**3** for 40 min at room temperature and pelleted by centrifugation, and cell-associated radioactivity was quantified by scintillation counting. [³⁵S]-**3** binding was measured on K562 cells in TBS alone (no divalent cation) (□), TBS plus 5 mM EDTA (▨), TBS plus 1 mM Ca^{2+} and 1 mM Mg^{2+} (shaded bar), or TBS plus 1 mM Mn^{2+} (■).

The residue was HPLC-purified to obtain 27 mg (0.34 mmol) of **4b** (48% yield). Ion spray mass spectrum of **4b**: 804.7 Da (theoretical), 805.6 Da [$M + H$] (observed).

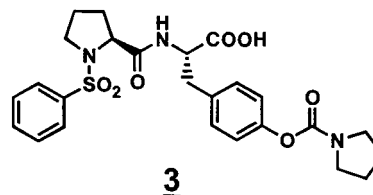
Cross-Linking of [¹²⁵I]-4a to $\alpha 4\beta 1$ on Cells and on Purified $\alpha 4\beta 1$ and $\alpha 9\beta 1$. [¹²⁵I]-**4a** cross-linking was tested on cells expressing $\alpha 1\beta 1$, $\alpha 2\beta 1$, $\alpha 4\beta 1$, and $\alpha 6\beta 1$. Cells (0.5×10^7) were suspended in 100 μ L of 10 mM Hepes, pH 7.5, 150 mM NaCl, and 2 mM glucose (binding buffer) containing 1 mM Ca^{2+} and 1 mM Mg^{2+} , 1 mM Ca^{2+} and 1 mM Mg^{2+} plus 1 μ g/mL mAb TS2/16, or 1 mM Mn^{2+} . [¹²⁵I]-**4a** was added to the cells to a final concentration of 5 nM, and they were incubated in the dark for 60 min at 23 °C. The samples were then exposed to long-wave ultraviolet 366 nm light for 10 min. The cells were washed two times with binding buffer containing 1 mM Ca^{2+} and 1 mM Mg^{2+} and lysed in buffer containing 1% Triton X-100. After 30 min at 4 °C, particulates were removed by centrifugation at top speed for 20 min at 4 °C in an Eppendorf centrifuge. The cell lysates were mixed with reducing SDS sample buffer, boiled, and subjected to SDS-PAGE on a 4–20% gradient gel. The gel was dried and exposed to X-ray film.

Aliquots (15 μ L) of purified $\alpha 4\beta 1$ or purified $\alpha 9\beta 1$, each containing 25 μ g/mL integrin in 50 mM Hepes, pH 7.5, 150 mM NaCl, 0.025% Triton X-100, 25 nM [¹²⁵I]-**4a**, 1 mM $CaCl_2$, and 1 mM $MgCl_2$, were incubated at 23 °C for 40 min and exposed to ultraviolet light at 366 nm for 5 min. Samples were analyzed by SDS-PAGE and exposed to

X-ray film. Pieces of gel containing the iodinated bands were excised with a razor blade and then further analyzed by CNBr peptide mapping as previously described (61). Cross-linking of [¹²⁵I]-**4b** to purified $\alpha 4\beta 1$ and $\alpha 9\beta 1$ was performed following the same protocol.

RESULTS AND DISCUSSION

Identification of *N*-(Benzenesulfonyl)-(L)-prolyl-(L)-O-(1-pyrrolidinylcarbonyl)tyrosine (3**) as a High-Affinity Ligand for $\alpha 9\beta 1$.** Compound **3** was identified as a potent inhibitor of the Mn^{2+} -activated $\alpha 4\beta 1$ ($IC_{50} = 0.14$ nM) from a structure-activity relationship analysis of small molecule inhibitors of the integrin (62). Like many other $\alpha 4\beta 1$ inhibitors, **3** also recognized the related integrin $\alpha 4\beta 7$, which shares many of the same ligands as $\alpha 4\beta 1$. The IC_{50} of **3** for Mn^{2+} -activated $\alpha 4\beta 7$ was 2.8 nM in these assays (62), indicating that it is >100-fold more potent as an inhibitor of $\alpha 4\beta 1$ than of $\alpha 4\beta 7$. As expected, the inhibitor is a more potent inhibitor of $\alpha 4\beta 7$ than of other integrins that were evaluated, including $\alpha 1\beta 1$, $\alpha 2\beta 1$, $\alpha 5\beta 1$, and $\alpha IIB\beta 3$ (see Table 1).



Recent studies have demonstrated (46, 54, 55) that integrin $\alpha 9\beta 1$ shares many of the same ligands as $\alpha 4\beta 1$, raising the possibility that it might also bind **3**. To directly answer the question of selectivity for $\alpha 9\beta 1$, we generated an $\alpha 9$ -transfected K562 cell line, analogous to the K562 lines described previously for other $\beta 1$ integrins, and tested the binding of **3** to this cell line. To facilitate the analysis of binding, a radiolabeled version of **3** was prepared in which the [³⁵S]sulfonamide moiety was incorporated during the synthesis of the compound. Binding of [³⁵S]-**3** to the $\alpha 9$ -transfected K562 cell line was dependent on divalent cations, consistent with the known metal ion requirements of integrin function (Figure 1). Binding buffers containing 1 mM Mn^{2+} or 1 mM Ca^{2+} plus 1 mM Mg^{2+} supported the binding of **3** to the $\alpha 9$ -K562 cells, while no binding was observed in TBS buffer alone or in TBS plus EDTA (Figure 1). [³⁵S]-**3** binding could be competed with a 100-fold excess of unlabeled **3** (see below). Similar characteristics were found for the binding of **3** to $\alpha 4$ -transfected K562 cells (Figure 1). A low but significant level of binding was seen on the $\alpha 2$ -

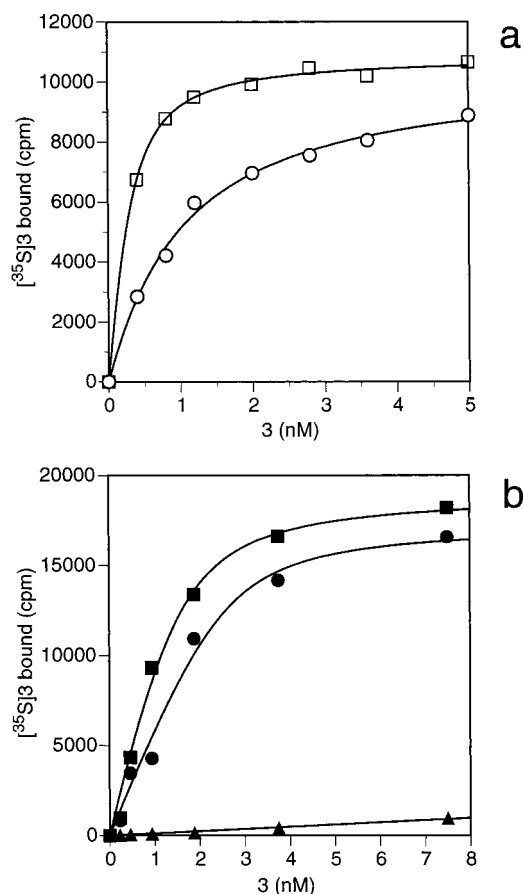


FIGURE 2: Binding of $[^{35}\text{S}]\text{-3}$ to cells expressing $\alpha 4 \beta 1$ or $\alpha 9 \beta 1$ under activating (1 mM Mn^{2+}) and nonactivating (1 mM Ca^{2+} , 1 mM Mg^{2+}) conditions. (a) Jurkat cells at $1.0 \times 10^6/\text{mL}$ or (b) $\alpha 9$ -transfected K562 cells at $3.0 \times 10^6/\text{mL}$ were incubated at room temperature for 30 min with the indicated concentrations of $[^{35}\text{S}]\text{-3}$ in the presence of TBS plus 1 mM Mn^{2+} on $\alpha 4 \beta 1$ cells (□) or $\alpha 9 \beta 1$ cells (■), TBS plus 1 mM Ca^{2+} and 1 mM Mg^{2+} on $\alpha 4 \beta 1$ cells (○) or $\alpha 9 \beta 1$ cells (●), or TBS alone (no divalent cations) (▲) on $\alpha 9 \beta 1$ cells. The cells were then pelleted by centrifugation, and cell-associated radioactivity was quantified by scintillation counting. Solid lines represent the best fit of the data to a quadratic binding equation.

transfected K562 cells in the presence of 1 mM Mn^{2+} (Figure 1), which is consistent with the low affinity of **3** for $\alpha 2 \beta 1$ (Table 1). No significant binding was observed on $\alpha 1$ -transfected K562 cells. Figure 2 shows the binding of $[^{35}\text{S}]\text{-3}$ to Jurkat ($\alpha 4 \beta 1$ positive) and $\alpha 9$ -transfected K562 cells under Mn^{2+} -activated conditions and under nonactivating conditions represented by binding in the presence of 1 mM Ca^{2+} plus 1 mM Mg^{2+} . $[^{35}\text{S}]\text{-3}$ binding curves were dose-dependent and saturable. From the binding data, ED_{50} values of about 0.15 and 1 nM were observed for binding to Jurkat cells and 0.75 and 1 nM for binding to $\alpha 9$ -K562 cells in 1 mM Mn^{2+} and 1 mM Ca^{2+} plus 1 mM Mg^{2+} , respectively. Using the number of specific counts of $[^{35}\text{S}]\text{-3}$ bound at saturation to estimate receptor number, the $\alpha 9$ -K562 cells contain approximately 100000 copies of $\alpha 9 \beta 1/\text{cell}$, and the Jurkat cells contain approximately 75000 copies of $\alpha 4 \beta 1/\text{cell}$.

Because $\alpha 9 \beta 1$ is found on neutrophils, we also tested for the binding of $[^{35}\text{S}]\text{-3}$ to freshly isolated human PMNs. Since neutrophils contain low but functional levels of $\alpha 4 \beta 1$ (55), the cells were pretreated with the selective $\alpha 4 \beta 1$ inhibitor BIO5192 (28; K_D of BIO5192 in 1 mM Ca^{2+} and 1 mM

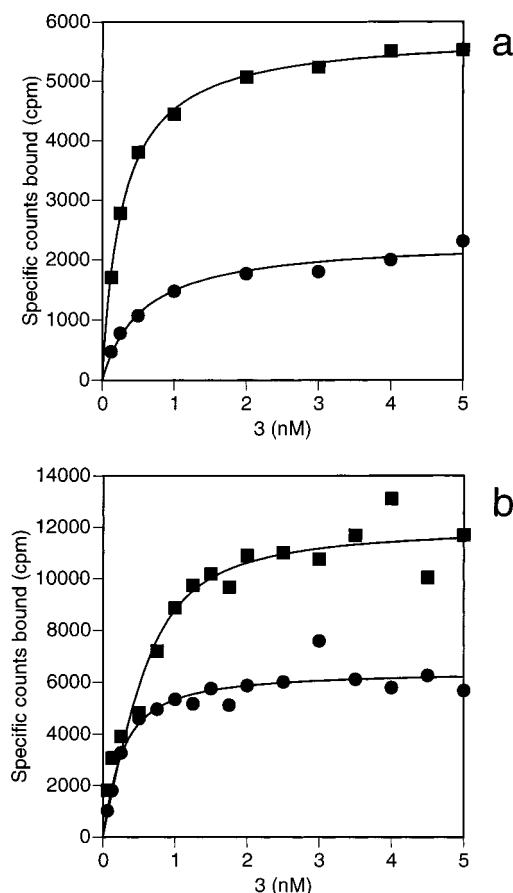


FIGURE 3: Binding of $[^{35}\text{S}]\text{-3}$ to PMNs and G-361 cells. Neutrophils at $1.0 \times 10^7/\text{mL}$ (a) or G-361 cells at $1.0 \times 10^6/\text{mL}$ (b) were incubated at 37°C for 60 min with the indicated concentrations of $[^{35}\text{S}]\text{-3}$ in the presence of binding buffer plus 1 mM Mn^{2+} (■) or binding buffer plus 1 mM Ca^{2+} and 1 mM Mg^{2+} (●). The cells were collected by filtration and washed, and cell-associated radioactivity was quantified by scintillation counting. Solid lines represent the best fit of the data to a hyperbolic equation.

Mg^{2+} is $<10 \text{ pM}$ for $\alpha 4 \beta 1$ and is 500 nM for $\alpha 9 \beta 1$ under the same conditions). Binding of $[^{35}\text{S}]\text{-3}$ to $\alpha 9 \beta 1$ on PMNs was dose-dependent and saturable (Figure 3a). The ED_{50} was approximately 0.28 nM in 1 mM Mn^{2+} and 0.56 nM in 1 mM Ca^{2+} plus 1 mM Mg^{2+} . Assuming that all of the binding observed in 1 mM Mn^{2+} is due to $\alpha 9 \beta 1$, then the number of binding sites detected was ~ 2500 receptors/cell. Treatment with PMA caused a slight increase in receptor number but had no effect on ED_{50} for either activation state (data not shown).

Finally, we tested for binding of $[^{35}\text{S}]\text{-3}$ to the G-361 human cancer cell line, which is known to express relatively high levels of $\alpha 9 \beta 1$ (Figure 3b). Again binding was dose-dependent and saturable. The ED_{50} was approximately 0.5 nM for both the 1 mM Mn^{2+} and the 1 mM Ca^{2+} plus 1 mM Mg^{2+} states. The maximum number of counts bound in 1 mM Mn^{2+} corresponds to ~ 50000 binding sites/cell. The substantially smaller number of **3** binding sites on G-361 cells and neutrophils in 1 mM Ca^{2+} plus 1 mM Mg^{2+} versus in 1 mM Mn^{2+} probably reflects, at least in part, the dissociation of bound **3** from the lower affinity 1 mM Ca^{2+} plus 1 mM Mg^{2+} state during the wash step in the filtration protocol that was used for these measurements. This effect was not observed in binding data on $\alpha 9$ -transfected K562 cells (Figure 2), where the cells were processed by the

centrifugation method without a wash step. The possibility that some of the additional counts seen in the 1 mM Mn^{2+} state might be due to **3** binding to other integrins cannot be ruled out. However, if this is happening, the affinity for binding to these additional sites is indistinguishable from that for binding to $\alpha 9\beta 1$ as binding conformed to a single-site model. On neutrophils in particular, the binding of **3** to $\alpha \text{D}\beta 2$ will need to be investigated, since $\alpha \text{D}\beta 2$ has also been shown to be able to bind VCAM-1 (65).

The quadratic shape of some of the binding curves in Figure 2 suggested that the K_D for binding was small compared to the concentration of integrin present in the binding assays. Consequently, a kinetic assessment was used to establish actual affinities of **3** for $\alpha 4\beta 1$ and for $\alpha 9\beta 1$. Kinetic measurements for the binding of **3** to $\alpha 4\beta 1$ on Jurkat cells and $\alpha 9\beta 1$ on $\alpha 9$ -transfected K562 cells are shown in Figure 4a and Table 2. Binding to both integrins was rapid, with k_{on} values equaling $1.9 \times 10^6 \text{ M}^{-1} \text{ s}^{-1}$ for $\alpha 4\beta 1$ in 1 mM Mn^{2+} , $2.6 \times 10^6 \text{ M}^{-1} \text{ s}^{-1}$ for $\alpha 4\beta 1$ in 1 mM Ca^{2+} and 1 mM Mg^{2+} , $3.5 \times 10^6 \text{ M}^{-1} \text{ s}^{-1}$ for $\alpha 9\beta 1$ in 1 mM Mn^{2+} , and $4 \times 10^6 \text{ M}^{-1} \text{ s}^{-1}$ for $\alpha 9\beta 1$ in 1 mM Ca^{2+} and 1 mM Mg^{2+} . These findings indicate that the activation state of $\alpha 4\beta 1$ does not greatly influence the association rate for binding, although we consistently observed a slight increase in the association rate for the nonactivated integrin. Association rate constants of similar magnitude were reported previously for the $\alpha 4\beta 1$ binding of the small molecule inhibitors BIO1211 (16) and BIO7662 (28). Dissociation curves for binding of [^{35}S]-**3** to $\alpha 9\beta 1$ and to $\alpha 4\beta 1$ under the various states of activation are shown in Figure 4b (rate constants are listed in Table 2). Dissociation from $\alpha 9\beta 1$ in the presence of 1 mM Mn^{2+} is too slow to allow determination of an accurate k_{off} , but extrapolation from the available data suggests a half-life for dissociation of at least 15 h, corresponding to a $k_{\text{off}} \leq 0.1 \times 10^{-4} \text{ s}^{-1}$. Since $k_{\text{on}} = 3.5 \times 10^6 \text{ M}^{-1} \text{ s}^{-1}$, the resulting K_D that was calculated from k_{on} and k_{off} is 3 pM or less. Thus, while dose-dependent and saturable binding was observed using equilibrium measurements (see Figure 1), the molar concentration of $\alpha 4\beta 1$ in this assay greatly exceeded the K_D for binding. Consequently, the binding curves were in essence simply measuring a titration of the receptor to full occupancy, and the ED_{50} values observed do not correspond to the binding affinity. This problem has been well documented in previous binding studies using BIO1211 (16) and BIO7662 (28). The dissociation rate in the presence of 1 mM Mn^{2+} for $\alpha 4\beta 1$ is slightly faster than for $\alpha 9\beta 1$, with an estimated k_{off} of $\leq 0.1 \times 10^{-4} \text{ s}^{-1}$. Since $k_{\text{on}} = 2 \times 10^6 \text{ M}^{-1} \text{ s}^{-1}$, the resulting K_D that was calculated from k_{on} and k_{off} is $\leq 5 \text{ pM}$ for binding to $\alpha 4\beta 1$ under these conditions. k_{off} for the 1 mM Ca^{2+} , 1 mM Mg^{2+} nonactivated state of the $\alpha 9\beta 1$ was $7.2 \times 10^{-4} \text{ s}^{-1}$, corresponding to a K_D of 180 pM, and for $\alpha 4\beta 1$ was $k_{\text{off}} = 19 \times 10^{-4} \text{ s}^{-1}$, corresponding to a K_D of 730 pM. As a result of the very slow dissociation of **3** from the Mn^{2+} -activated integrins, it was not possible to determine if the dissociation curves were monophasic or biphasic. Dissociation from the 1 mM Ca^{2+} , 1 mM Mg^{2+} state appeared to be monophasic for both integrins.

The affinity of **3** for $\alpha 4\beta 1$ was evaluated under a more extensive set of conditions to better compare its binding properties with the previously published binding data for BIO1211 (16, 28). First, when EDTA was added to Jurkat

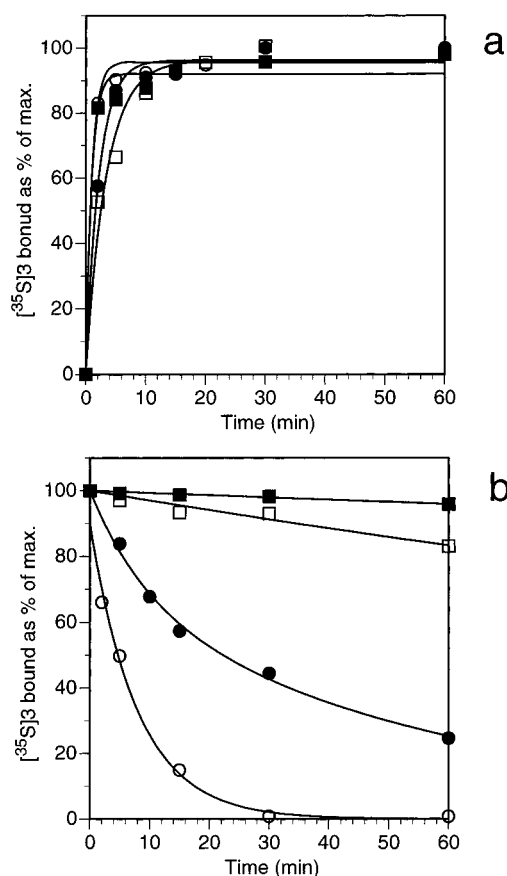


FIGURE 4: Assessing binding of [^{35}S]-**3** to cells using kinetic measurements. On- and off-rates for the binding of [^{35}S]-**3** to Jurkat cells ($1 \times 10^6/\text{mL}$) and $\alpha 9$ -transfected K562 cells ($3.0 \times 10^6/\text{mL}$) were determined in the presence of TBS plus 1 mM Mn^{2+} and $\alpha 9\beta 1$ cells (■) or $\alpha 4\beta 1$ cells (□) or TBS containing 1 mM Ca^{2+} and 1 mM Mg^{2+} and $\alpha 9\beta 1$ cells (●) or $\alpha 4\beta 1$ cells (○). For on-rate measurements (a), cells were treated with 2 nM [^{35}S]-**3** for 2.5, 5, 10, 15, 20, 30, or 60 min, collected by centrifugation, and subjected to scintillation counting. The data were fitted to an exponential equation by nonlinear regression. For off-rates (b), cells were treated with 5 nM [^{35}S]-**3** for 40 min. 500 nM unlabeled **3** was added, and the cells were further incubated for the times indicated in the presence of divalent cation. Cells were pelleted at each time point, and cell-associated [^{35}S]-**3** was measured by scintillation counting. Dissociation data are represented as a percent of the maximum total counts bound as a function of time. The data were fitted to a single exponential for all curves. k_{on} and k_{off} values were calculated from the curve fits. k_{off} is the observed dissociation rate constant; k_{on} is the observed association rate constant divided by the concentration of **3**. Data shown are from a single determination of the on- and off-rates.

cells that had been first treated with Mn^{2+} and [^{35}S]-**3**, radioactivity was released slowly from the **3**– $\alpha 4\beta 1$ complex ($k_{\text{off}} = \leq 0.1 \times 10^{-4} \text{ s}^{-1}$ in 1 mM Mn^{2+} versus $0.42 \times 10^{-4} \text{ s}^{-1}$ in Mn^{2+} plus EDTA) (see Table 3). In fact, less than half of the bound [^{35}S]-**3** was released after 3 h of treatment with EDTA. Thus, while binding of [^{35}S]-**3** to $\alpha 4\beta 1$ is dependent on the presence of divalent cation, the small molecule–integrin complex is relatively stable to the EDTA treatment. EDTA treatment had a similar effect on BIO1211 binding on Jurkat cells that had been first treated with Mn^{2+} and BIO1211 ($k_{\text{off}} = 1.4 \times 10^{-4} \text{ s}^{-1}$ in 1 mM Mn^{2+} versus $15 \times 10^{-4} \text{ s}^{-1}$ in Mn^{2+} plus EDTA). Second, we measured the effects of the activating mAb TS2/16 on **3** binding under various conditions (see Tables 2 and 3). The dissociation of **3** from $\alpha 4\beta 1$ in 1 mM Ca^{2+} and 1 mM Mg^{2+} that had been

Table 2: Binding of Compound **3** to Jurkat and $\alpha 9$ -Transfected K562 Cells under Various States of Activation^a

buffer	$k_{on}/10^6$ ($M^{-1} s^{-1}$)	$k_{off}/10^{-4}$ (s^{-1})	K_D (pM)
Jurkat cells ^b			
1 mM Ca^{2+} , 1 mM Mg^{2+}	2.6	19	730
1 mM Mn^{2+}	1.9	≤ 0.1	≤ 5
1 mM Ca^{2+} , 1 mM Mg^{2+} + TS2/16	2.0	2.3	120
10 mM Mg^{2+}	1.8	0.36	20
$\alpha 9$ -K562 cells			
1 mM Ca^{2+} , 1 mM Mg^{2+}	4.0	7.2	180
1 mM Mn^{2+}	3.5	≤ 0.1	≤ 3
1 mM Ca^{2+} , 1 mM Mg^{2+} + TS2/16	2.0	1.1	55
10 mM Mg^{2+}	0.83	0.7	84

^a On-rates, off-rates, and K_D values for the binding of [³⁵S]-**3** to $\alpha 4 \beta 1$ and $\alpha 9 \beta 1$ were determined from kinetic measurements as described in Figure 4. ^b The dissociation of **3** from $\alpha 4 \beta 1$ showed an initial burst that accounted for $\leq 15\%$ of the total bound counts. The reported k_{off} value is based on the slow phase of dissociation that accounted for $\geq 85\%$ of bound counts.

Table 3: Dissociation of Compound **3** from Jurkat Cells under Various States of Activation^a

buffer	$k_{off}/10^{-4}$ (s^{-1})	
	compound 3	BIO1211
1 mM Ca^{2+} , 1 mM Mg^{2+}	19 ^b	> 140
1 mM Ca^{2+} , 1 mM Mg^{2+} , TS2/16	2.3 ^b	5.1
1 mM Mn^{2+}	≤ 0.1 ^b	1.4
1 mM Mn^{2+} , TS2/16	≤ 0.08 ^b	0.17
1 mM Mn^{2+} \rightarrow 5 mM EDTA	0.42	15
10 mM Mg^{2+}	0.36 ^b	5.3
10 mM Mg^{2+} , TS2/16	≤ 0.1 ^b	0.40
2 mM Mg^{2+}	0.72	8.3
2 mM Mg^{2+} , TS2/16	0.22	0.76
0.5 mM Mg^{2+}	1.7	
0.5 mM Mg^{2+} , TS2/16	0.58	
1 mM Ca^{2+}	120 ^c	
1 mM Ca^{2+} , TS2/16	6.2 ^c	

^a Off-rate values for the binding of [³⁵S]-**3** to $\alpha 4 \beta 1$ on Jurkat cells were determined from kinetic measurements as described in Figure 4. Corresponding BIO1211 data (16) are shown for comparative purposes.

^b Dissociation showed an initial burst that accounted for $\leq 15\%$ of the total bound counts. The reported k_{off} value is based on the slow phase of dissociation that accounted for $\geq 85\%$ of bound counts. ^c Dissociation appeared biphasic with the fast phase accounting for 26% and 29% of the bound counts for the 1 mM Ca^{2+} and 1 mM Ca^{2+} , TS2/16 states, respectively. Reported k_{off} values are derived from a double-exponential curve fit and correspond in each case to the rate constant governing the dissociation of the majority ($\geq 70\%$) of bound counts.

exposed to the mAb was 8-fold slower than that observed in the absence of the mAb, suggesting that affinity of **3** for TS2/16-activated $\alpha 4 \beta 1$ is higher. Measurable effects of TS2/16 with Mg^{2+} added were observed at all Mg^{2+} concentrations tested. There was no evidence that the combination of TS2/16 plus Mn^{2+} stabilized the **3**-integrin complex to a greater degree than was seen with Mn^{2+} alone. The dissociation rates from the Mn^{2+} alone and Mn^{2+} plus TS2/16 are too slow to accurately assess this point. Following TS2/16 treatment, larger shifts in BIO1211 dissociation rates were observed under the corresponding conditions than for **3**. The clear differences in the magnitudes of the effects of TS2/16 on **3** and BIO1211 binding presumably reflect differences in the way the small molecules interact with the integrin and point to differences in their association with the $\beta 1$ -chain. Third, we tested the dependence of Ca^{2+} on binding (see

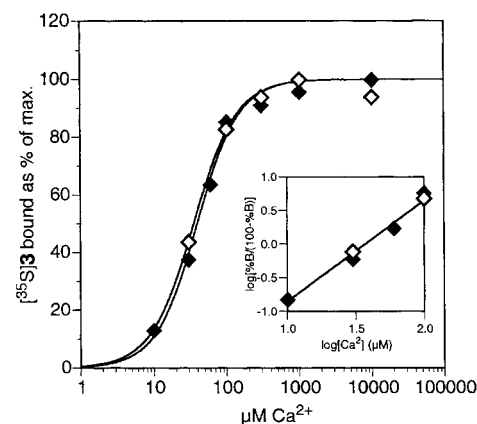


FIGURE 5: Ca^{2+} dependence of [³⁵S]-**3** binding. 1 mL Jurkat cells at 1×10^6 /mL (\diamond) or $\alpha 9$ -transfected K562 cells (\blacklozenge) at 3.0×10^6 /mL were incubated at room temperature for 40 min with 3 nM [³⁵S]-**3** in TBS containing the indicated concentrations of Ca^{2+} . The cells were then pelleted by centrifugation, and cell-associated radioactivity was quantified by scintillation counting. The insert shows the data from 10 to 100 μM Ca^{2+} linearized in the form of a Hill plot (% B is the amount of **3** bound as a % of the maximum).

Figure 5). Much lower concentrations of Ca^{2+} were needed to promote the binding of **3** to $\alpha 4 \beta 1$ than those needed to promote the binding of BIO1211 to $\alpha 4 \beta 1$ (16) (EC_{50} for **3** binding was 30 μM Ca^{2+} versus > 10 mM Ca^{2+} for BIO1211 binding). The shift in the Ca^{2+} dependence of **3** binding supports the recently proposed coupled equilibrium model for ligand and metal ion binding to $\alpha 4 \beta 1$ (28), in which the relatively high affinity of **3** for $\alpha 4 \beta 1$ lowers the metal ion concentration needed to promote ligand binding.

Modulation of the 9EG7 LIBS Epitope by 3. Ligand binding and integrin activation induce a cascade of conformational changes within the integrin that ultimately leads to the activation of intracellular signaling pathways. These changes have been studied in detail using mAbs whose epitopes are either exposed (termed LIBS, also referred to as CLIBS due to modulation of the epitope by cations; 63) or lost following ligand binding (13, 64). **3** is a LIBS inducer (Figure 6) and therefore might be expected to exhibit the same profile of effects natural ligands exhibit (16, 51, 61). While **3** induced the LIBS epitope on both $\alpha 4 \beta 1$ and $\alpha 9 \beta 1$, the binding of the two integrins to 9EG7 in the absence of ligand was clearly different. For $\alpha 4 \beta 1$, Mg^{2+} treatment promoted binding as is apparent by the signal seen in the absence of **3**. No binding was seen with $\alpha 9 \beta 1$ under the same conditions. A second difference in the titration curves is that about a 10-fold lower level of **3** is needed for half-maximal induction of $\alpha 4 \beta 1$ cell binding than for the $\alpha 9 \beta 1$ cells. This finding was surprising since the affinity of **3** for $\alpha 9 \beta 1$ was greater than the affinity for $\alpha 4 \beta 1$ under most activation states that were tested (see Table 2). Interestingly, in these measurements of K_D , only in Mg^{2+} was the affinity of **3** for $\alpha 9 \beta 1$ lower than the affinity for $\alpha 4 \beta 1$.

Bazzoni et al. (63) have found through a direct comparison of divalent cation- and ligand-induced conformational changes for five different $\beta 1$ integrins ($\alpha 2 \beta 1$, $\alpha 3 \beta 1$, $\alpha 4 \beta 1$, $\alpha 5 \beta 1$, and $\alpha 6 \beta 1$) that the mechanisms for regulating function were quite divergent. In particular, they observed by monitoring the effects of EGTA on binding that EGTA inhibited LIBS induction on $\alpha 4 \beta 1$, promoted LIBS expression on $\alpha 2 \beta 1$, $\alpha 5 \beta 1$, and $\alpha 6 \beta 1$, and had no effect on the LIBS epitope on

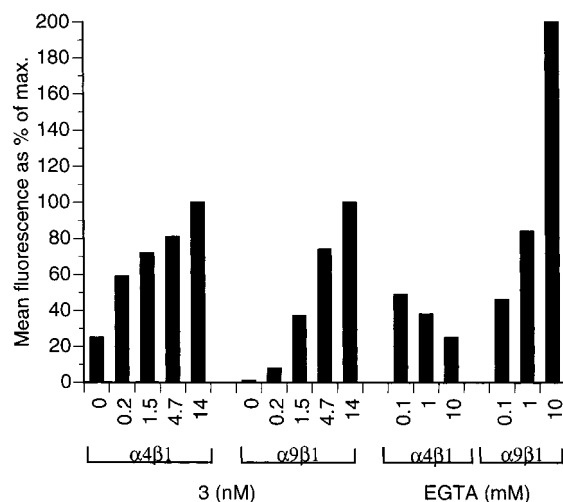


FIGURE 6: Induction of the expression of the 9EG7 LIBS epitope by **3**. The effects of **3** on the expression of the LIBS epitope that can be detected with the 9EG7 mAb were evaluated on cells expressing $\alpha 9\beta 1$ and $\alpha 4\beta 1$ in an adhesion assay. $\alpha 9$ -K562 cells and Jurkat cells were labeled with calcein for 30 min at room temperature, washed with TBS, and suspended at 4×10^6 cells/mL in TBS + 2 mM Mg^{2+} . The labeled cells were incubated for 30 min at 37 °C with serial dilutions of unlabeled **3** or EGTA at the concentrations indicated in 96-well Costar Easywash plates that had been coated with 10 μ g/mL 9EG7 and blocked with bovine serum albumin. Plates were washed three times and read on a CytoFluor 4000 multi well plate reader from PerSeptive Biosystems (excitation at 485 nm, emission at 530 nm). For $\alpha 4\beta 1$ cells background binding was 400 mean fluorescence units and maximum binding was 11000 units, and for $\alpha 9\beta 1$ cells background binding was 500 mean fluorescence units and maximum binding was 2300 units. 0% = nonspecific binding to non-9EG7 coated wells. 100% = binding seen in the presence of 14 nM **3**. As a further control for LIBS induction certain wells were treated with Mn^{2+} , which itself is a potent inducer of the LIBS epitope. As expected, Mn^{2+} induced expression of the LIBS epitope on both cell types.

$\alpha 3\beta 1$. As previously observed (63), we also found that EGTA inhibited LIBS induction on $\alpha 4\beta 1$ (Figure 6). In contrast, treatment of $\alpha 9$ -K562 cells with EGTA promoted LIBS induction on $\alpha 9\beta 1$ (Figure 6), producing even a greater increase in binding than was seen following **3** treatment. The high concentration of EGTA needed to elicit a response suggests that its effect is on a bound Ca^{2+} , which is not readily accessible to the added chelator. Evidence for such a Ca^{2+} binding site on $\alpha 4\beta 1$ was previously reported (28). As part of the LIBS studies, we also treated the $\alpha 9$ -K562 and Jurkat cells with 1 mM Ca^{2+} . No binding of 9EG7 to $\alpha 9\beta 1$ occurred in the 1 mM Ca^{2+} state, whereas 9EG7 binding to $\alpha 4\beta 1$ in 1 mM Ca^{2+} occurred at a level that was similar to the level seen in Mg^{2+} (data not shown). These observations further support the notion that bound Ca^{2+} on $\alpha 9\beta 1$ is affecting the presentation of the LIBS epitope. Although the significance of the differences in the response of 9EG7 binding is unknown, it points to possible differences in the regulation of $\alpha 4\beta 1$ and $\alpha 9\beta 1$ by metal ions.

Measuring Metal Ion and Ligand Binding with [^{35}S]-3** as a Reporter.** The regulation of ligand binding by metal ions is complex and is not fully understood (12–14). Integrins typically contain three to five metal ion binding sites (12, 66), and binding is cooperative (4, 28). The [^{35}S]-**3** binding data shown in Figures 1 and 2 clearly demonstrate the metal ion dependence of **3** binding under both activating and nonactivating conditions. Since Ca^{2+} can stimulate binding

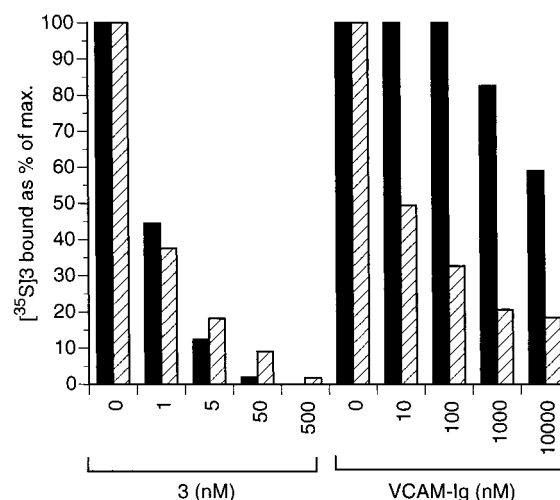


FIGURE 7: Analysis of VCAM-1 binding through competition. The binding of **3** and VCAM-Ig to $\alpha 9\beta 1$ (■) or $\alpha 4\beta 1$ (▨) was assessed on $\alpha 9$ -K562 cells or Jurkat cells through competition with [^{35}S]-**3**. 0.5 mL of $\alpha 9$ -K562 cells (3×10^6 cells/mL) or Jurkat cells (1×10^6 cells/mL) in TBS + 1 mM Mn^{2+} buffer was incubated for 30 min at room temperature with serial dilutions of unlabeled **3** or VCAM-Ig (8) at the concentrations indicated. At the end of the incubation, 5 nM [^{35}S]-**3** was added, and the cells were further incubated for 5 min. The cells were then pelleted, and bound [^{35}S]-**3** was quantified by scintillation counting. The binding data show bound counts as a percent of maximum counts bound with no competitor, plotted against the competitor concentration.

of some ligands to some integrins and inhibit binding for others (12, 14, 15), we were particularly interested in the effects of Ca^{2+} on **3** binding. The data shown in Figure 5 clearly demonstrate that Ca^{2+} promotes the binding of **3** to $\alpha 4\beta 1$ and $\alpha 9\beta 1$ and that in each case the EC_{50} for binding in the presence of 3 nM **3** is 30 μ M Ca^{2+} . The Ca^{2+} dependence of the binding of **3** to both integrins indicates that metal ion binding is cooperative, with a Hill coefficient of $n_H = 1.5$. These findings identify further similarities in the regulation of $\alpha 4\beta 1$ and $\alpha 9\beta 1$ function. Previously, we observed that ligand and metal ion binding to $\alpha 4\beta 1$ were regulated through a coupled equilibrium and, therefore, that the metal ion dependence of ligand binding was coupled to the affinity of the ligand for the integrin (28). Consequently, for the high-affinity ligand BIO7662 ($K_D = 3$ pM in 1 mM Ca^{2+} and 1 mM Mg^{2+}), the EC_{50} for Ca^{2+} -dependent binding of BIO7662 to $\alpha 4\beta 1$ was low (5–10 μ M), and for the lower affinity ligand BIO1211 ($K_D = 20$ –40 nM for $\alpha 4\beta 1$ in 1 mM Ca^{2+} and 1 mM Mg^{2+}), the EC_{50} for Ca^{2+} -dependent binding was high (>10 mM). For **3**, which is of intermediate affinity ($K_D = 0.9$ nM for $\alpha 4\beta 1$ in 1 mM Ca^{2+} and 1 mM Mg^{2+}), the EC_{50} for Ca^{2+} -dependent binding of **3** to $\alpha 4\beta 1$, 30 μ M Ca^{2+} , is intermediate to the values seen with BIO7662 and BIO1211, further supporting the model. We can infer from the low EC_{50} for the Ca^{2+} -dependent binding of **3** to $\alpha 9\beta 1$ (30 μ M Ca^{2+}) that ligand and metal ion binding to $\alpha 9\beta 1$ are also regulated through a coupled equilibrium.

Recently, several studies demonstrated that both $\alpha 9\beta 1$ and $\alpha 4\beta 1$ bound VCAM-1 and osteopontin as ligands (45, 46, 55, 67). To better understand the interactions of $\alpha 9\beta 1$ and $\alpha 4\beta 1$ with these ligands, binding to VCAM-1 and osteopontin was evaluated using **3** as a probe in a competition format. Binding of VCAM-1 to cells expressing the integrins was performed in solution (Figure 7). The cells were first

incubated with serial dilutions of VCAM-Ig, and then [35 S]-**3** was added as a reporter to measure remaining free integrin. As expected, **3** competed with VCAM-Ig binding with both integrins; however, the apparent affinity of VCAM-Ig for $\alpha 4 \beta 1$ of 10 nM was at least 1000 times greater than the apparent affinity of VCAM-Ig for $\alpha 9 \beta 1$ of $\geq 10 \mu\text{M}$. While the biological significance of the different affinities for VCAM-1 is not known, the interaction of $\alpha 9 \beta 1$ with VCAM-1 is clearly of functional significance (55). Nevertheless, the binding data demonstrate that the ligand binding pockets on $\alpha 9 \beta 1$ and $\alpha 4 \beta 1$ are quite different in their interactions with this natural ligand.

The effects of **3** on the binding of $\alpha 9 \beta 1$ and $\alpha 4 \beta 1$ to osteopontin were evaluated in an adhesion format. A recombinant version of the N-terminal thrombin fragment of osteopontin (OPN 10N) (68), containing amino acid residues 17–168 of the human osteopontin sequence, was used as the ligand as previously described (68, 69). The 96-well plates were coated with the recombinant osteopontin fragment, and binding of the integrin-expressing cells to the osteopontin was performed as previously described (68) except that we used fluorescently labeled cells instead of crystal violet staining to facilitate quantitation of the binding. Results from these analyses are presented in Figure 8. Binding was first tested in buffer containing 1 mM Ca^{2+} and 1 mM Mg^{2+} (Figure 8a). As expected on the basis of published data for the binding of $\alpha 4 \beta 1$ to OPN 10N (45), Jurkat cells readily bound the osteopontin-coated plates, and the binding could be blocked with the anti- $\alpha 4$ neutralizing mAb HP1/2. All of the specific binding could be competed with the antibody, indicating that adhesion of the Jurkat cells to OPN 10N was all through $\alpha 4 \beta 1$. Compound **3** was an effective inhibitor of the adhesion with an IC_{50} of 0.06 nM. As a further control for selectivity, inhibition of binding was measured using the highly selective $\alpha 4 \beta 1$ inhibitor BIO7662 (28). Like **3**, BIO7662 also inhibited Jurkat cell binding but with an IC_{50} of 0.03 nM.

When the same analysis was performed on $\alpha 9$ -K562 cells, no binding of the cells to OPN 10N was observed in buffer containing 1 mM Ca^{2+} and 1 mM Mg^{2+} . We have no explanation for this finding since others have reported binding of $\alpha 9$ -expressing cells to OPN 10N under these conditions (54, 67, 68) and we followed the protocol from one of these publications (67). However, binding of $\alpha 9$ -K562 cells to OPN 10N was readily observed in the presence of Mn^{2+} , and the binding was blocked with the anti- $\alpha 9$ neutralizing mAb Y9A2 (Figure 8b). All of the specific binding was inhibited, indicating that adhesion of the $\alpha 9$ -K562 cells to osteopontin was all via $\alpha 9 \beta 1$. Compound **3** was an effective inhibitor of the adhesion with an IC_{50} of 0.2 nM. BIO7662 also inhibited binding but with an IC_{50} of 50 nM, consistent with previous estimates for the affinity of BIO7662 for Mn^{2+} -activated $\alpha 9 \beta 1$ (no binding to $\alpha 9 \beta 1$ under nonactivating conditions was detected using [35 S]-BIO7662 as a probe). The binding of Jurkat cells to OPN 10N in 1 mM Mn^{2+} was also inhibited by **3** and BIO7662 (Figure 8b). As expected, BIO7662 was much more effective as an inhibitor for $\alpha 4 \beta 1$ than for $\alpha 9 \beta 1$, as evident by the 250-fold difference in the IC_{50} values on Jurkat and $\alpha 9$ -K562 cells, while the IC_{50} for **3** binding to Jurkat cells was slightly higher than for **3** binding to $\alpha 9$ -K562 cells. When binding to cells was performed in solution under the conditions used

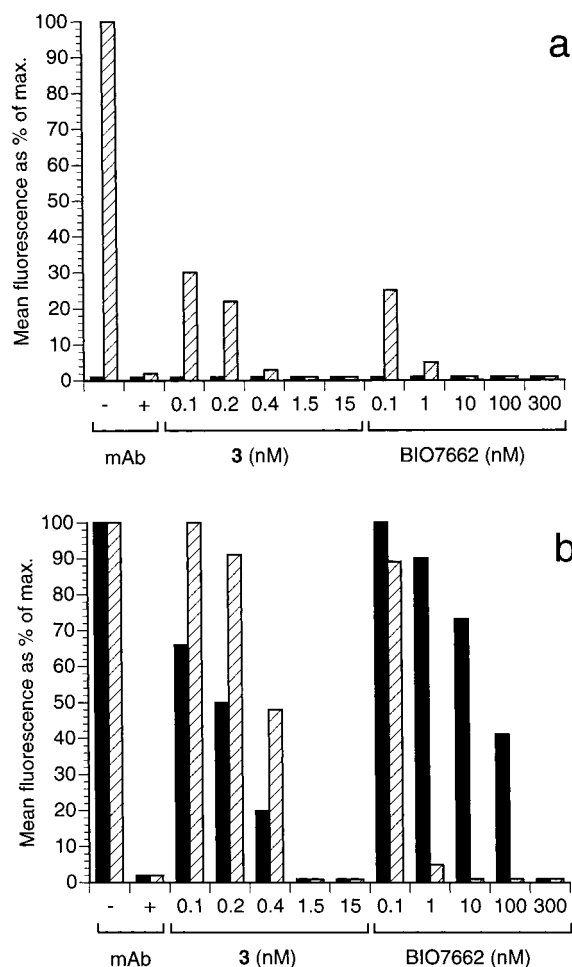
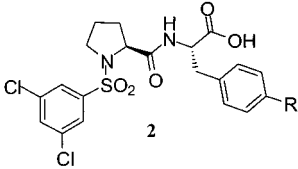
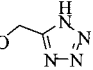
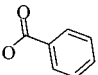
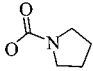
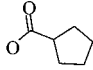
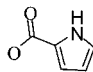


FIGURE 8: Analysis of osteopontin binding through competition. The effects of **3** and BIO7662 on the binding of $\alpha 9 \beta 1$ (■) or $\alpha 4 \beta 1$ (□) to osteopontin were assessed in an adhesion assay. Calcein-labeled $\alpha 9$ -K562 cells (4×10^6 cells/mL) or Jurkat cells (4×10^6 cells/mL) in TBS + 1 mM Ca^{2+} and 1 mM Mg^{2+} (a) or in TBS + 1 mM Mn^{2+} (b) were incubated for 30 min at 37 °C with serial dilutions of unlabeled **3** or BIO7662 (28) at the concentrations indicated in 96-well Costar Easywash plates that had been coated with 1 $\mu\text{g/mL}$ OPN 10N and blocked with bovine serum albumin. For the binding of Jurkat cells in Mn^{2+} , the coating concentration of OPN 10N was 0.03 $\mu\text{g/mL}$. Plates were washed three times and read on a CytoFluor 4000 multi well plate reader from PerSeptive Biosystems (excitation at 485 nm, emission at 530 nm). For binding to osteopontin in Mn^{2+} , it was necessary to include 100 μM GRGDSP peptide in the binding buffer to prevent adhesion of the cells through $\alpha 5 \beta 1$. Specificity of binding was tested by treating cells with 10 $\mu\text{g/mL}$ neutralizing mAb HP1/2 for the analysis of $\alpha 4 \beta 1$ binding and mAb Y9A2 (Chemicon) for the analysis of $\alpha 9 \beta 1$ binding.

in Figure 7, no binding of OPN 10N to $\alpha 9 \beta 1$ or $\alpha 4 \beta 1$ was observed at concentrations of OPN 10N up to 100 μM (data not shown). Although we could not directly measure the affinity of osteopontin for $\alpha 9 \beta 1$ or $\alpha 4 \beta 1$ in these studies, we can infer that the affinity for $\alpha 9 \beta 1$ is significantly lower, since binding in the adhesion format was only observed in Mn^{2+} , while binding to $\alpha 4 \beta 1$ did not require integrin activation. These findings indicate that **3** is a potent inhibitor of the interactions of $\alpha 4 \beta 1$ both with VCAM-1 and with osteopontin and of the interactions of $\alpha 9 \beta 1$ with these same ligands. Recently, Marcinkiewicz et al. (54) proposed the presence of a second ligand binding site on $\alpha 9 \beta 1$ on the basis of the observation that a peptide derived from osteopontin was able to compete with osteopontin but did not

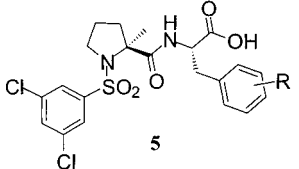
Table 4: Evaluation of the Ligand Binding Properties of $\alpha 9\beta 1$ through SAR^a


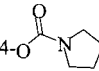
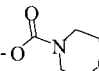
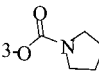
Compds	R	$\alpha 4\beta 1$ IC ₅₀ , nM	$\alpha 9\beta 1$ IC ₅₀ , nM	$\alpha 4\beta 7$ IC ₅₀ , nM
2a	OH	0.34	77	820
2b	OCH ₃	0.37	7.8	360
2c	O- <i>t</i> -(C ₄ H ₉)	0.21	4.3	120
2d	O(CH ₂) ₃ CH ₃	1.1	37	300
2e	OCH ₂ C ₆ H ₅	1.9	150	850
2f	O(CH ₂) ₂ OCH ₃	0.28	6.7	62
2g	OCH ₂ CN	0.26	8.1	250
2h		0.21	2.8	170
2i	OCH ₂ COCH ₃	0.18	28	51
2j	OCH ₂ CO ₂ - <i>t</i> -(C ₄ H ₉)	0.13	65	210
2k		0.45	15	43
2l		0.13	3	1.9
2m		0.22	21	59
2n		0.26	4.5	13

^a G-361 cells (1×10^5 cells/well) in binding buffer plus 100 nM BIO5192 were added to Millipore Unifilter plates containing 1 mM Mn²⁺, 200 pM [³⁵S]-**3**, and the test compound in binding buffer. The plates were incubated at 37 °C for 60 min. Cells were collected by filtration and washed, and cell-associated radioactivity was quantified by scintillation counting. Corresponding data for the binding of [¹²⁵I]VCAM-Ig to $\alpha 4\beta 1$ on Jurkat cells and to $\alpha 4\beta 7$ on RPMI-8866 cells (62) are shown for comparative analysis.

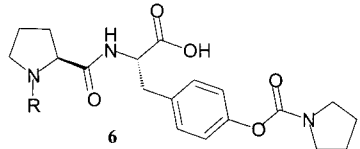
compete with VCAM-1 for binding to the integrin. We see no evidence for a second ligand binding site on $\alpha 9\beta 1$ using **3** as a competitor of osteopontin and VCAM-1 binding. More extensive binding studies will be needed to resolve this issue.

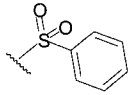
Analysis of Ligand Binding by Monitoring Structure–Activity Relationships. As an independent approach to probe for potential differences in the $\alpha 9\beta 1$ and $\alpha 4\beta 1$ ligand binding sites, the structure–activity relationships (SAR) of a series of related inhibitors were evaluated, which originally had been characterized in an attempt to isolate potent selective $\alpha 4\beta 1$ inhibitors (62) and at that time had been characterized for selectivity toward $\alpha 4\beta 7$. Results from these analyses are summarized in Tables 4–6. The 26 compounds shown all share similar structural features with **3** (compound **6a** in Table 6) and allow us to investigate the structural features of the small molecule that make it such a potent inhibitor of $\alpha 9\beta 1$. The three primary binding domains on **3** from left to right are the benzenesulfonyl moiety, the central (L)-proline, and the terminal 4-substituted (L)-phenylalanine. The carboxy terminus is thought to mimic an aspartic acid, which is found in all ligands that bind to these integrins. The first series of

Table 5: Evaluation of the Ligand Binding Properties of $\alpha 9\beta 1$ through SAR^a


Compds	R	$\alpha 4\beta 1$ IC ₅₀ , nM	$\alpha 9\beta 1$ IC ₅₀ , nM	$\alpha 4\beta 7$ IC ₅₀ , nM
5a	4-O- <i>t</i> -(C ₄ H ₉)	0.27	1800	650
5b		0.17	2.3	5.3
5c	4-OC(O)N(CH ₂ CH ₃) ₂	0.19	6.9	30
5d	4-OC(O)N(<i>i</i> -Pr) ₂	0.22	11	62
5e	4-OC(O)N(CH ₃)(C ₆ H ₅)	0.25	11	12
5f		0.13	8.4	3.5
5g	3-O- <i>t</i> -(C ₄ H ₉)	1.8	490	>100
5h	3-OCH ₂ CO ₂ - <i>t</i> -(C ₄ H ₉)	0.41	1200	>100
5i		3.6	1100	>100

^a G-361 cells (1×10^5 cells/well) in binding buffer plus 100 nM BIO5192 were added to Millipore Unifilter plates containing 1 mM Mn²⁺, 200 pM [³⁵S]-**3**, and the test compound in binding buffer. The plates were incubated at 37 °C for 60 min. Cells were collected by filtration and washed, and cell-associated radioactivity was quantified by scintillation counting. Corresponding data for the binding of [¹²⁵I]VCAM-Ig to $\alpha 4\beta 1$ on Jurkat cells and to $\alpha 4\beta 7$ on RPMI-8866 cells (62) are shown for comparative analysis.

Table 6: Evaluation of the Ligand Binding Properties of $\alpha 9\beta 1$ through SAR^a


Compds	R	$\alpha 4\beta 1$ IC ₅₀ , nM	$\alpha 9\beta 1$ IC ₅₀ , nM	$\alpha 4\beta 7$ IC ₅₀ , nM
6a		0.14	1.1	2.8
6b	SO ₂ CH ₃	0.5	150	4.4
6c	H	25	inactive	inactive

^a G-361 cells (1×10^5 cells/well) in binding buffer plus 100 nM BIO5192 were added to Millipore Unifilter plates containing 1 mM Mn²⁺, 200 pM [³⁵S]-**3**, and the test compound in binding buffer. The plates were incubated at 37 °C for 60 min. Cells were collected by filtration and washed, and cell-associated radioactivity was quantified by scintillation counting. Corresponding data for the binding of [¹²⁵I]VCAM-Ig to $\alpha 4\beta 1$ on Jurkat cells and to $\alpha 4\beta 7$ on RPMI-8866 cells (62) are shown for comparative analysis.

compounds (Table 4) shows the effects of 4' substitutions on the phenylalanine ring. Differences in their potency for

$\alpha 9\beta 1$, ranging from 3 to 150 nM, were observed. Most significant was the 10-fold increase in potency in going from the hydroxy substitution (**2a**, $IC_{50} = 77$ nM) to the methoxy function (**2b**, $IC_{50} = 7.8$ nM). The same substitution had no effect on binding to $\alpha 4\beta 1$ and produced only a 2-fold increase in affinity for $\alpha 4\beta 7$. Slight further increases in affinity for $\alpha 9\beta 1$ occurred for the four larger substitutions seen with compounds **2c**, **2h**, **2l**, and **2n**. All other substitutions caused a decrease in potency. None of the substitutions in Table 4 had any significant effects on $\alpha 4\beta 1$ binding, though, like with $\alpha 9\beta 1$, they had dramatic effects on binding to $\alpha 4\beta 7$. Although the overall trends of the substitutions were similar for $\alpha 9\beta 1$ and $\alpha 4\beta 7$, the effects of the substitutions were slightly larger on $\alpha 4\beta 7$.

Table 5 shows 3' and 4' benzene substitutions on a related framework in which proline was replaced with 1-methylproline. Compound **5b**, which corresponds to **2l** in the proline series, was most active toward $\alpha 9\beta 1$ ($IC_{50} = 2.3$ nM), while **5a**, which corresponds to **2c** in the proline series, was least active ($IC_{50} = 1800$ nM). Interestingly, whereas the IC_{50} values of **5b** and **2l** for $\alpha 9\beta 1$ were similar, the relative activities of **5a** and **2c** for $\alpha 9\beta 1$ differed by 420-fold. All other 4' substitutions in the 1-methylproline series had little or no effect on activity. In contrast, there were no significant differences in the IC_{50} values of **5a**, **5b**, **2c**, or **2l** toward $\alpha 4\beta 1$, and for $\alpha 4\beta 7$, while large differences were seen for **5a** and **5b**, the IC_{50} value of 650 nM for **5a** represented only a 4.5-fold drop in activity of **2c** on $\alpha 4\beta 7$. The 3' substitutions in compounds **5g**, **5h**, and **5i** provided a look at the effects of ring position on activity. For compound **5b** ($IC_{50} = 2.3$ nM on $\alpha 9\beta 1$) the corresponding 3' substitution (**5i**) had an $IC_{50} = 1100$ nM, while for **5a** the corresponding 3' substitution (**5g**) was slightly more active. Similarly, when compared to **2c**, **2j**, and **2l** in the proline series, the potencies of **5g**, **5h**, and **5i** for $\alpha 9\beta 1$ were reduced by > 100 fold. Thus there is a significant positional effect of the phenyl ring substituents on potency. As in the proline series, similar trends in the affinity for binding of the methylproline series to $\alpha 4\beta 7$ were observed. For $\alpha 4\beta 1$ binding, the 3' substitutions resulted in only slight decreases in potency, and the 4' substitutions revealed minor fluctuations.

The effects of the benzenesulfonyl group on the potency of **3** for $\alpha 9\beta 1$ were particularly striking (see Table 6). Replacement of the benzenesulfonyl function seen in **6a** with a methanesulfonyl group (**6b**) caused a 140-fold drop in potency toward $\alpha 9\beta 1$ from 1.1 to 150 nM, while the affinities for $\alpha 4\beta 1$ and $\alpha 4\beta 7$ were reduced by only 2–3-fold by this substitution. When the benzenesulfonyl group was removed entirely (**6c**), no binding to $\alpha 9\beta 1$ and $\alpha 4\beta 7$ was observed, and the affinity for $\alpha 4\beta 1$ was reduced to 25 nM. The addition of the dichloro substitution to the benzene (**2l**) reduced the potency for $\alpha 9\beta 1$ by 3-fold, whereas it caused slight increases in potency for $\alpha 4\beta 1$ and $\alpha 4\beta 7$.

Although we might have expected from the SAR analysis that the ligand binding site on $\alpha 9\beta 1$ might resemble $\alpha 4\beta 1$ since it shares the same $\beta 1$ chain, or that the binding data for $\alpha 4\beta 1$ and $\alpha 4\beta 7$ might be similar since they share the same $\alpha 4$ chain, the binding data shown in Tables 4–6 reveal that the three integrins are quite distinct in their requirements for binding of this class of inhibitors. These findings indicate that both integrin chains contribute to **3** binding. The recent success in crystallizing $\alpha v\beta 3$ (**2l**) raises the possibility that

other integrin structures will soon follow. The high affinity of the **3** family for multiple integrins makes it an attractive target for cocrystallization studies. In characterizing the SAR for the 26 inhibitors shown in Tables 4–6, the [^{125}I]VCAM–Ig probe that was used for assessing binding to $\alpha 4\beta 1$ and $\alpha 4\beta 7$ could not be used in the $\alpha 9\beta 1$ study because of its low affinity for $\alpha 9\beta 1$. Consequently, the [^{35}S]–**3** probe was substituted for these analyses. While **3** is a competitive inhibitor of VCAM–Ig binding (Figure 7) and both bind the ligand binding pocket, the absolute IC_{50} values for the three data sets are not directly comparable.

The fact that so many of the $\alpha 4\beta 1$ inhibitors we characterized are potent inhibitors of $\alpha 9\beta 1$ raises the possibility that many of the $\alpha 4\beta 1$ inhibitors described elsewhere may also inhibit $\alpha 9\beta 1$ function. It is clear that in vitro and in vivo experiments with $\alpha 4\beta 1$ or $\alpha 4\beta 7$ small molecule inhibitors must be interpreted with caution, and evaluation of $\alpha 9\beta 1$ binding will be needed as part of any analysis of integrin specificity, at least with respect to compounds that bind $\alpha 4\beta 1$ or $\alpha 4\beta 7$. The wide cellular distribution of $\alpha 9\beta 1$ makes this point particularly significant. Currently, no neutralizing antibodies are available that can be used to assess $\alpha 9\beta 1$ function in animals. The availability of potent selective $\alpha 9\beta 1$ inhibitors should assist in this analysis.

Assessing 3–Integrin Interactions by Chemical Cross-Linking. To further investigate the nature of the interaction of **3** with $\alpha 9\beta 1$ and $\alpha 4\beta 1$, we used chemical cross-linking to covalently attach the small molecule to the integrin, and the reaction products were characterized by SDS–PAGE. A modified version of **3**, which contained a photoreactive azidophenyl moiety attached to the proline ring, was used for the cross-linking. The modified inhibitor is designated **4a**. The azidophenyl moiety was selected to also provide a site for iodination. [^{125}I]–Labeled **4a** cross-linking was tested on cells expressing $\alpha 1\beta 1$, $\alpha 2\beta 1$, $\alpha 4\beta 1$, and $\alpha 6\beta 1$ in buffer containing 1 mM Ca^{2+} plus 1 mM Mg^{2+} ; 1 mM Ca^{2+} , 1 mM Mg^{2+} , and 1 $\mu g/mL$ mAb TS2/16; or 1 mM Mn^{2+} (Figure 9a). The cells were suspended in 100 μL of binding buffer, incubated with [^{125}I]–**4a** for 60 min in the dark at 23 $^{\circ}C$, and then exposed to long-wavelength (366 nm) ultraviolet light for 10 min. The cells were washed twice with 1 mM Ca^{2+} plus 1 mM Mg^{2+} binding buffer, lysed, subjected to SDS–PAGE, and analyzed by autoradiography. Under the conditions tested, [^{125}I]–**4a** was cross-linked only to the $\alpha 4$ chain in $\alpha 4\beta 1$ cells and not to either the α - or β -chain of $\alpha 1\beta 1$, $\alpha 2\beta 1$, and $\alpha 6\beta 1$. The minor band at 150 kDa corresponds to the intact $\alpha 4$ chain, while the prominent band at 80 kDa corresponds to the N-terminal fragment of the $\alpha 4$ chain. As expected, most of the $\alpha 4$ -chain in K562 cells is proteolytically cleaved between R⁵⁵⁸ and S⁵⁵⁹ into the 80 kDa (N-terminal) and the 70 kDa (C-terminal) fragment, which are noncovalently associated (70). This cleavage event does not affect $\alpha 4\beta 1$ function (70). Addition of 1 mM Mn^{2+} decreased the amount of cross-linking relative to what we observed in 1 mM Ca^{2+} plus 1 mM Mg^{2+} alone or in 1 mM Ca^{2+} and 1 mM Mg^{2+} plus 1 $\mu g/mL$ mAb TS2/16 (Figure 9a).

Cross-linking with [^{125}I]–**4a** was also performed on purified $\alpha 4\beta 1$. When the cross-linking was run in the 1 mM Ca^{2+} plus 1 mM Mg^{2+} buffer, the ^{125}I -labeled 80 kDa $\alpha 4$ band again was the primary cross-linked product detected (Figure 9b, lane j). Cross-linking to a 150 kDa band and a 180 kDa

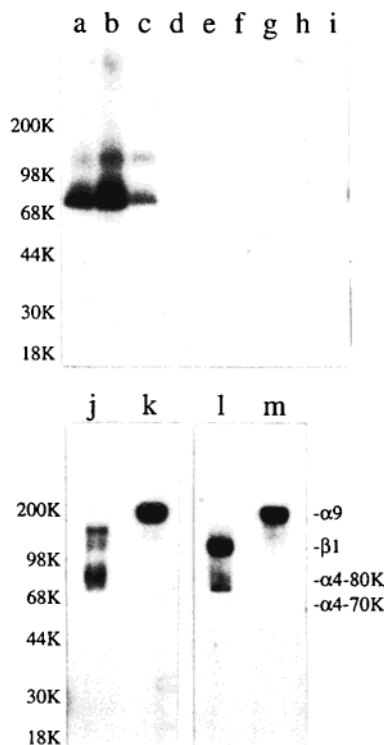


FIGURE 9: Analysis of integrin/small molecule interactions by photoaffinity cross-linking. (a) K562 cells expressing $\alpha 4\beta 1$ (lanes a–c), $\alpha 1\beta 1$ (lanes d–f), or $\alpha 6\beta 1$ (lanes g–i) in the presence of 1 mM Ca^{2+} and 1 mM Mg^{2+} (lanes a, d, and g), 1 mM Ca^{2+} and 1 mM Mg^{2+} plus 1 $\mu\text{g}/\text{mL}$ TS2/16 (lanes b, e, and h), or 1 mM Mn^{2+} (lanes c, f, and i) were incubated for 60 min at 23 °C in the dark with [^{125}I]-**4a** and then in 366 nm UV light for 10 min. Cells were washed and subjected to SDS–PAGE, and the radioactive small molecule was detected by autoradiography. (b) Affinity-purified $\alpha 4\beta 1$ (lanes j and l) and $\alpha 9\beta 1$ (lanes k and m) in TBS containing 1 mM Ca^{2+} and 1 mM Mg^{2+} were treated with [^{125}I]-**4a** (lanes j and k) or [^{125}I]-**4b** (lanes l and m) and analyzed by SDS–PAGE.

band was also observed but in lower amounts. The 150, 180, and 80 kDa bands were all characterized by peptide mapping using partial digestion with CNBr to generate a profile of cleavage products. By peptide mapping, the 150 and 180 kDa bands were clearly related to the 80 kDa $\alpha 4$ band (Figure 10c shows cleavage data for the 80 and 150 kDa bands). While the 150 and 180 kDa $\alpha 4$ bands have been previously described and the 150 kDa band is known to represent the intact $\alpha 4$ chain, the structure of the 180 kDa form is unknown (71).

The [^{125}I]-**4a** linkage within the 80 kDa fragment of the $\alpha 4$ -chain was further localized by CNBr mapping using the same method described previously for analyzing BIO1494– $\alpha 4\beta 1$ cross-linked products (61). Figure 10a shows the position of methionines within the $\alpha 4$ –80 kDa chain sequence. The theoretical and observed profiles derived from the cross-linking are presented in panels b and c of Figure 10, respectively. When the BIO1494– $\alpha 4$ 80 kDa chain cleavage map was analyzed by this method (61), the observed profile of masses (30, 40, 45, 55, 70, and 76 kDa) (data shown in lanes e and f of Figure 10c for comparative purposes) agreed well with the hypothetical pattern for CNBr fragment 1 (26, 39, 45, 54, 70, and 81 kDa) (Figure 10b, lane 1), indicating that cross-linked BIO1494 was localized within CNBr fragment 1 (residues 1–180) in the $\alpha 4$ -chain sequence. The series of fragments represent CNBr fragment

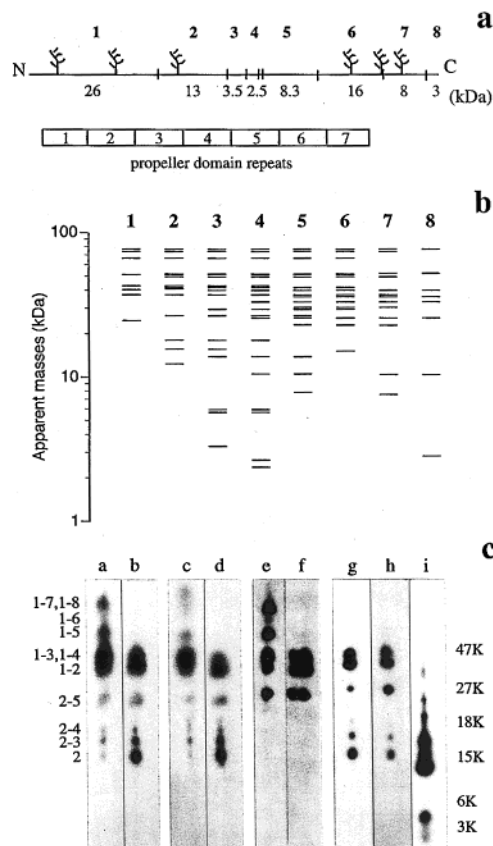


FIGURE 10: Analysis of the $\alpha 4\beta 1$ –small molecule cross-linked complex by CNBr mapping. The 80 kDa $\alpha 4$ -chain (residues 1–558 of the mature $\alpha 4$ -chain sequence) contains eight internal methionine residues. The schematic in panel a marks the positions of Met residues as perpendicular lines within the 80 kDa $\alpha 4$ -chain sequence. Specific CNBr fragments are marked numerically, where 1 denotes the N-terminal fragment and 8 denotes the C-terminal fragment. Potential glycosylation sites are marked by tree-like symbols. Theoretical masses indicated include an additional 3 kDa per glycosylation site. The box structure at the base of the sequence indicates the locations of the seven repeat domains from the propeller motif. Panel b shows theoretical partial cleavage profiles for each of the eight major CNBr fragments indicated in panel a, using the masses shown in panel a to generate the theoretical maps. For panel c, gel slices containing **4a**– and **4b**– $\alpha 4\beta 1$ -chain complexes were incubated with CNBr and subjected to SDS–PAGE on a 10–20% gradient gel as previously described (61). Cross-linked cleavage products were detected by autoradiography. Lanes a, c, and e, 7 mg/mL CNBr for 1 h; lanes b, d, and f–i, 70 mg/mL CNBr for 1 h. Lanes a and b, 80 kDa $\alpha 4$ -chain and [^{125}I]-**4a**; lanes c and d, 150 kDa $\alpha 4$ -chain and [^{125}I]-**4a**; lanes e and f, 80 kDa $\alpha 4$ -chain and BIO1494-DSS (61); lane g, 80 kDa $\alpha 4$ -chain and [^{125}I]-**4a**; lane h, 80 kDa $\alpha 4$ -chain and [^{125}I]-**4b**; lane i, 150 kDa $\beta 1$ -chain and [^{125}I]-**4b**. The positions of molecular mass standards are indicated at the right. Designations at the left indicate relevant fragment compositions for the **4a**–80 kDa $\alpha 4$ -chain cleavage fragments.

1 alone (26 kDa), fragment 1 + 2 (39 kDa), fragment 1–3 and/or 1–4 (43/45 kDa), fragment 1–5 (54 kDa), fragment 1–6 (70 kDa), and fragment 1–7 and/or 1–8 (78/81 kDa). The cleavage profiles for the **4a**– $\alpha 4$ 80 kDa chain conjugate (Figure 10c, lanes a and b) are similar to the profiles of the BIO1494– $\alpha 4$ 80 kDa chain conjugate (Figure 10c, lanes e and f) but contain three additional lower molecular weight fragments with masses of 19, 17, and 15 kDa that are absent from the BIO1494 analysis. Since these results are best represented by the theoretical pattern seen in Figure 10b, lane 2, which contains fragments with masses of 19, 16.5,

and 13 kDa, we can infer that the linkage is within CNBr fragment 2 (residues 181–264 in the mature $\alpha 4$ sequence). Further evidence for this conclusion came from the comparative analysis of the CNBr cleavage profiles of the 80 kDa (Figure 10c, lanes a and b) and the 150 kDa (Figure 10c, lanes c and d) bands. The only apparent difference in the profiles is in the loss of the 80 kDa band corresponding to CNBr fragments 1–7 and 1–8 in the analysis of the 150 kDa band and its replacement with a band of slightly higher mass, about 100 kDa. Cleavage at methionine residue 620 or 624 could account for this shift in mass. Furthermore, if the cross-link were further from the N-terminus, a more significant difference in the profiles would have occurred. The recently solved crystal structure for $\alpha \nu \beta 3$ (21) has provided a model for the ligand binding pocket on this integrin that presumably will be similar in other integrins as well. In this model, the ligand binding pocket is formed by blades 2 and 3 of the propeller domain on the α -chain and the MIDAS site in the A-domain of the β -chain. The residue 181–264 sequence contains blade 3 of the propeller domain in the $\alpha 4$ 80 kDa chain (Figure 10a), and therefore mapping of the **4a**– $\alpha 4$ 80 kDa chain linkage to CNBr fragment 2 supports this model for the ligand binding site (21).

When purified $\alpha 9\beta 1$ was subjected to cross-linking with [^{125}I]-**4a**, only the 200 kDa, $\alpha 9$ -chain was labeled with the probe (Figure 9b, lane k). No cross-linking to the $\beta 1$ -chain was observed. Thus both $\alpha 9\beta 1$ and $\alpha 4\beta 1$ are cross-linked within their α -chains when treated with **4a**. Because of the lack of reagents for characterizing $\alpha 9$ cleavage products, and the added complexity of the analysis due to the larger number of methionines in the $\alpha 9$ -chain, the cross-linked 200 kDa $\alpha 9$ -chain was not subjected to the mapping analysis.

In addition to the **4a** probe, a second cross-linker was synthesized, **4b**, in which the phenylazido moiety was attached to the meta position of the benzene ring on the benzenesulfonamide via an aminohexylamine linker. When this reagent was subjected to cross-linking on purified $\alpha 9\beta 1$ and $\alpha 4\beta 1$, $\alpha 9\beta 1$ (Figure 9, lane m) was again cross-linked on the 200 kDa $\alpha 9$ -chain. Most of $\alpha 4\beta 1$ cross-linking was now on the $\beta 1$ -chain (Figure 9, lane l), suggesting that the inhibitor might be oriented differently in the $\alpha 9\beta 1$ and $\alpha 4\beta 1$ ligand binding pockets. However, because the azido moiety in **4b** is attached to a hexylamine linker, the differences in the cross-linking patterns on $\alpha 9\beta 1$ and $\alpha 4\beta 1$ could simply reflect flexibility around the linker. In light of the structure of the ligand binding pocket (21), the hexylamine linker could easily allow **4b** to form linkages with sites on the α - and β -chains without changing its orientation in the pocket. When the **4a** and **4b** cross-linked $\alpha 4$ 80 kDa chain products were subjected to CNBr mapping, the cleavage profiles were identical (Figure 10, lanes g and h), supporting the notion that they are oriented similarly within the intact $\alpha 4\beta 1$. The cleavage profile for the **4b**– $\beta 1$ -chain cross-linked product (Figure 10c, lane i) was clearly distinct from the cleavage profile of the $\alpha 4$ cleavage products but matched exactly with the CNBr cleavage profile previously published for the BIO1494–ANB–NOS– $\beta 1$ -chain conjugate (61). Since the site of the BIO1494–ANB–NOS cross-link was previously localized to within the sequence DLSYSM (residues 130–136) in the $\beta 1$ -chain, we can infer that one of the contact points between **4b** and $\alpha 4\beta 1$ is at or near the MIDAS site in the $\beta 1$ A-domain.

With the solution of the $\alpha \nu \beta 3$ crystal structure, the data have provided the first definitive view of how integrin α - and β -chains associate to form a ligand binding pocket. The **4a** and **4b** cross-linking data verify that compound **3**-like inhibitors bind this region of $\alpha 4\beta 1$ and, together with the crystal data, provide a picture of how **3** might interact with the integrin. By superimposing the $\alpha 9\beta 1$ and $\alpha 4\beta 1$ sequences on the coordinates of $\alpha \nu \beta 3$, it should be possible to use the cross-linking and the SAR data to build a better understanding of structural features within the ligand binding pockets of $\alpha 9\beta 1$ and $\alpha 4\beta 1$ that govern ligand binding and account for the differences in SAR. One unexpected feature of the $\alpha \nu \beta 3$ crystal structure was the identification of a second metal ion binding site in the $\beta 1$ A-domain that is adjacent to the MIDAS site (referred to as the ADMIDAS site) (21). The ADMIDAS site was occupied with a Ca^{2+} ion in the $\alpha \nu \beta 3$ structure. However, since the ligand binding pocket was unoccupied, it is unclear how metal ion binding at this site and the MIDAS site regulates ligand binding. In studying the binding of BIO7662 to purified $\alpha 4\beta 1$ in the presence of radioactive Ca^{2+} (28), we previously detected two types of Ca^{2+} binding sites that can now be associated with the two sites observed in the crystal structure. One site was slowly occupied by the added Ca^{2+} ($t_{1/2} = 30$ min, site 2) probably in an exchange process, and Ca^{2+} binding to the site was shown to be independent of BIO7662 binding. In light of the $\alpha \nu \beta 3$ data, we can now conclude that site 2 represents binding of the Ca^{2+} at the ADMIDAS site since only the ADMIDAS was occupied with Ca^{2+} in the $\alpha \nu \beta 3$ structure. The other site was rapidly occupied by radioactive Ca^{2+} ($t_{1/2} < 5$ min, site 1), but only in the presence of BIO7662. We infer that site 1 binding represents the binding of Ca^{2+} at the MIDAS, which is consistent with **4b** cross-linking data. Since BIO7662 is a hybrid structure, containing key structural features of BIO1211 (16) and compound **3**, we tested if BIO1211 or **3** also caused this Ca^{2+} binding event. Compound **3** promoted rapid Ca^{2+} binding ($t_{1/2} < 5$ min), but unlike with BIO7662, there was no evidence for binding of the radioactive Ca^{2+} at a second site. Instead, bound ^{45}Ca reached a maximum after 10 min and then remained unchanged for the duration of the 2 h binding study. BIO1211 binding had no effect on ^{45}Ca binding. The Ca^{2+} binding data with BIO1211 added resembled binding seen in the absence of added ligand (i.e., binding at site 2). Thus BIO1211, BIO7662, and **3** exhibit very different effects with respect to this Ca^{2+} binding event. The compound **3** binding data were particularly surprising. One explanation for the data is that **3** stabilizes the metal ion bound at site 2, possibly by coordinating with the metal ion, and therefore is not susceptible to an exchange reaction with the ^{45}Ca . An alternative explanation would be that binding at site 1 results in the displacement of the metal ion at site 2 to give an integrin–**3** complex in which only site 1 is occupied by Ca^{2+} . Although it was not possible to distinguish between these alternatives from the limited data set, the availability of these three very different families of binders should facilitate future studies that are designed to address metal ion regulation of integrin function.

In summary, we have demonstrated that **3** is a potent inhibitor of $\alpha 9\beta 1$ and $\alpha 4\beta 1$ and can be used as a probe to investigate the biochemical properties of both integrins.

Binding data with [^{35}S]-**3** revealed very similar metal ion dependencies for the two integrins and similar patterns for modulation of affinity by activation. The affinity of **3** for both integrins was increased by addition of the TS2/16 antibody. Binding of **3** also induced the LIBS epitope, consistent with binding at the ligand binding site. The effects of the activating and LIBS antibodies on function indicate similar $\beta 1$ -chain function. One clear distinction in the LIBS study was that Ca^{2+} stimulated 9EG7 binding to $\alpha 4\beta 1$ but inhibited its binding to $\alpha 9\beta 1$. Cross-linking studies with **4a** demonstrated a direct association of the small molecule with the integrin α -chains, while studies with **4b** revealed that there were differences in the association of the ligands. Extensive SAR studies using natural and synthetic ligands identified further differences in the ligand binding pockets. When binding to VCAM-1 and osteopontin was evaluated, the affinity of $\alpha 4\beta 1$ for these natural ligands was much higher than that of $\alpha 9\beta 1$. These differences in structure and function will be reflected in distinct biologies of these integrins and can be exploited in the design of selective $\alpha 9\beta 1$ and $\alpha 4\beta 1$ inhibitors. As a soluble, monovalent probe for $\alpha 9\beta 1$ function, **3** represents a novel tool that should aid in further unraveling the complexities associated with integrin function.

ACKNOWLEDGMENT

We thank Francisco Sanchez-Madrid for the TS2/16 antibody, Martin Hemler for providing the $\alpha 2$ - and $\alpha 4$ -K562 transfectants and the B5G10 hybridoma, Dean Sheppard for the $\alpha 9$ cDNA, Arnoud Sonnenberg for the $\alpha 6$ -transfected K562 cells, Paul Weinreb for the various forms of osteopontin, and Philip Gotwals for providing the $\alpha 1$ -transfected K562 cell line. We also thank the other members of the Biogen-Merck VLA4 task force for helpful discussions.

REFERENCES

- Hynes, R. O. (1992) *Cell* 69, 11–25.
- Ruoslahti, E. (1991) *J. Clin. Invest.* 87, 1–5.
- Wayer, E. A., and Kovach, N. L. (1992) *J. Cell Biol.* 116, 489–497.
- Lobb, R. R., Antognetti, G., Pepinsky, R. B., Burkly, L., Leone, D., and Whitty, A. (1995) *Cell Adhes. Commun.* 3, 385–397.
- Pepinsky, B., Hession, C., Chen, L. L., Moy, P., Burkly, L., Jakobowski, A., Chow, E. P., Chi-Rosso, G., Luhowskyj, S., and Lobb, R. (1992) *J. Biol. Chem.* 267, 17820–17826.
- Dustin, M. L., Olive, D., and Springer, T. A. (1989) *J. Exp. Med.* 169, 503–517.
- Pepinsky, R. B., Chen, L. L., Meier, W., and Wallner, B. P. (1991) *J. Biol. Chem.* 266, 18244–18249.
- Jakubowski, A., Rosa, M. D., Bixler, S., Lobb, R., and Burkly, L. C. (1995) *Cell Adhes. Commun.* 3, 131–142.
- Chan, B. M. C., Wong, J. G. P., Rao, A., and Hemler, M. E. (1991) *J. Immunol.* 147, 398–404.
- Shimizu, Y., VanSeventer, G. A., Horgan, K. J., and Shaw, S. (1990) *Nature* 345, 250–253.
- Masumoto, A., and Hemler, M. E. (1993) *J. Biol. Chem.* 268, 228–234.
- Plow, E. F., Haas, T. A., Zhang, L., Loftus, J., and Smith, J. W. (2000) *J. Biol. Chem.* 275, 21785–21788.
- Humphries, M. J. (1996) *Cur. Opin. Cell Biol.* 8, 632–640.
- Hu, D. D., Barbas, C. F., III, and Smith, J. W. (1996) *J. Biol. Chem.* 271, 21745–21751.
- Mould, A. P., Akiyama, S. K., and Humphries, M. J. (1995) *J. Biol. Chem.* 270, 26270–26277.
- Chen, L. L., Whitty, A., Lobb, R. R., Adams, S. P., and Pepinsky, R. B. (1999) *J. Biol. Chem.* 274, 13167–13175.
- Leitinger, B., McDowall, A., Stanley, P., and Hogg, N. (2000) *Biochim. Biophys. Acta* 1498, 91–98.
- Gulino, D., Boudignon, C., Zhang, L., Concord, E., Rabiet, M.-J., and Margue, G. (1992) *J. Biol. Chem.* 267, 1001–1007.
- Springer, T. A. (1997) *Proc. Natl. Acad. Sci. U.S.A.* 94, 65–72.
- Irie, A., Kamata, T., and Takada, Y. (1997) *Proc. Natl. Acad. Sci. U.S.A.* 94, 7198–7203.
- Xiong, J.-P., Stehle, T., Diefenbach, B., Zhang, R., Dunker, R., Scott, D. L., Joachimiak, A., Goodman, S. L., and Arnaout, M. A. (2001) *Science* 294, 339–345.
- Corbi, A. L., Miller, L. J., O'Connor, K., Larson, R. S., and Springer, T. A. (1987) *EMBO J.* 6, 4023–4028.
- Tuckwell, D. S., and Humphries, M. J. (1997) *FEBS Lett.* 400, 297–303.
- Lee, J.-O., Rieu, P., Arnaout, A., and Liddington, R. (1995) *Cell* 80, 631–638.
- Qu, A., and Leahy, D. J. (1996) *Structure* 4, 931–942.
- Emsley, J., King, S. L., Bergelson, J. M., and Liddington, R. C. (1997) *J. Biol. Chem.* 272, 28512–28517.
- Nolte, M., Pepinsky, R. B., Venyaminov, S. Y., Kotliansky, V., Gotwals, P. J., and Karpusas, M. (1999) *FEBS Lett.* 452, 379–385.
- Chen, L. L., Whitty, A., Scott, D., Lee, W.-C., Cornebise, M., Adams, S. P., Petter, R. C., Lobb, R. R., and Pepinsky, R. B. (2001) *J. Biol. Chem.* 276, 36520–36529.
- Hemler, M. E., Elices, M. J., Parker, C., and Takada, Y. (1990) *Immunol. Rev.* 114, 45–65.
- Lobb, R. R., and Hemler, M. E. (1994) *J. Clin. Invest.* 94, 1722–1728.
- Springer, T. A. (1994) *Cell* 76, 301–314.
- Damle, N. K., and Aruffo, A. (1991) *Proc. Natl. Acad. Sci. U.S.A.* 88, 6403–6407.
- Anwar, A. R., Walsh, G. M., Cromwell, O., Kay, A. B., and Wardlaw, A. J. (1994) *Immunology* 82, 222–228.
- Clark, E. A., and Brugge, J. S. (1995) *Science* 268, 233–239.
- Udagawa, T., Woodside, D. G., and McIntyre, B. W. (1996) *J. Immunol.* 157, 1965–1972.
- Yoshikawa, H., Sakihama, T., Nakajima, Y., and Tasaka, K. (1996) *J. Immunol.* 156, 1832–1840.
- Ferguson, T. A., Mizutani, H., and Kupper, T. S. (1991) *Proc. Natl. Acad. Sci. U.S.A.* 88, 8072–8076.
- Wahl, S. M., Allen, J. B., Hines, K. L., Imamichi, T., Wahl, A. M., Furcht, L. T., and McCarthy, J. B. (1994) *J. Clin. Invest.* 94, 655–662.
- Molossi, S., Elices, M., Arrhenius, T., Diaz, R., Coulber, C., and Rabinovitch, M. (1995) *J. Clin. Invest.* 95, 2601–2610.
- Miller, D., Khan, O., Sheremata, W., Blumhardt, L., Rice, G., O'Connor, P., and the International Antigen MS Trial Group (2001) *Multiple Sclerosis* 7, S16.
- Osborn, L., Hession, C., Tizard, R., Vassalio, C., Luhowskyj, S., Chi-Rosso, G., and Lobb, R. (1989) *Cell* 59, 1203–1211.
- Elices, M. J., Osborn, L., Takada, Y., Crouse, C., Luhowskyj, S., Hemler, M. E., and Lobb, R. R. (1990) *Cell* 60, 577–584.
- Wayner, E. A., Garcia-Pardo, A., Humphries, M. J., McDonald, J. A., and Carter, W. G. (1989) *J. Cell Biol.* 109, 1321–1330.
- Guan, J. L., and Hynes, R. O. (1990) *Cell* 60, 53–61.
- Bayless, K. J., Meininger, G. A., Scholtz, J. M., and Davis, G. E. (1998) *J. Cell Sci.* 111, 1165–1174.
- Takahashi, H., Isobe, T., Horibe, S., Takagi, J., Yokosaki, Y., Sheppard, D., and Saito, Y. (2000) *J. Biol. Chem.* 275, 23589–23595.
- Wang, J.-H., Pepinsky, B., Stehle, T., Liu, J.-H., Karpusas, M., Browning, B., and Osborn, L. (1995) *Proc. Natl. Acad. Sci. U.S.A.* 92, 5714–5718.
- Vanderslice, P., Ren, K., Revelle, J. K., Kim, D. C., Scott, D., Bjercke, R. J., Yeh, E. T. H., Beck, P. J., and Kogan, T. P. (1997) *J. Immunol.* 158, 1710–1718.
- Jackson, D. Y., Quan, C., Artis, D. R., Rawson, T., Blackburn, B., Struble, M., Fitzgerald, Chui, H., Renz, M., Jones, S., and Fong, S. (1997) *J. Med. Chem.* 40, 3359–3368.
- Abraham, W. M., Ahmed, A., Sielczak, M. W., Narita, M., Arrhenius, T., and Elices, M. J. (1997) *Am. J. Respir. Crit. Care Med.* 156, 696–703.

51. Lin, K.-C., Ateeq, H. S., Hsiung, S. H., Chong, L. T., Zimmerman, C. N., Castro, A., Lee, W. C., Hammond, C. E., Kalkunte, S., Chen, L. L., Pepinsky, R. B., Leone, D. R., Sprague, A. G., Abraham, W. M., Gill, A., Lobb, R. R., and Adams, S. P. (1998) *J. Med. Chem.* 42, 920–934.
52. Dutta, A. S., Gormley, J. J., Coath, M., Hassall, L., Hayward, C. F., Gellert, P. R., Kittlety, R. S., Alcock, P. J., Ferguson, R., Halterman, T., Jamieson, A., Moors, J. A., Moores, J. M., Rees, A., Wood, L. J., Reilly, C. F., and Haworth, D. (2000) *J. Pept. Sci.* 6, 398–412.
53. Palmer, E. L., Ruegg, C., Ferrando, R., Pytela, R., and Sheppard, D. (1993) *J. Cell Biol.* 123, 1289–1297.
54. Marcinkiewicz, C., Taooka, Y., Yokosaki, Y., Calvete, J. J., Marcinkiewicz, M. M., Lobb, R. R., Niewiarowski, S., and Sheppard, D. (2000) *J. Biol. Chem.* 275, 31930–31937.
55. Taooka, Y., Chen, J., Yednock, T., and Sheppard, D. (1999) *J. Cell Biol.* 145, 413–420.
56. Young, B. A., Taooka, Y., Liu, S., Askins, K. J., Yokosaki, Y., Thomas, S. M., and Sheppard, D. (2001) *Mol. Biol. Cell.* 12, 3214–3225.
57. Shang, T., Yednock, T., and Issekutz, A. C. (1999) *J. Leukocyte Biol.* 66, 809–816.
58. Huang, X. Z., Wu, J. F., Ferrando, R., Lee, J. H., Wang, Y. L., Farese, R. V., Jr., and Sheppard, D. (2000) *Mol. Cell. Biol.* 20, 5208–5215.
59. Hanlon, W. A., Stolk, J., Davies, P., Humes, J. L., Mumford, R., and Bonney, R. J. (1991) *J. Leukocyte Biol.* 50, 43–48.
60. Makarem, R., Newham, P., Askari, J. A., Green, L. J., Clements, J., Edwards, M., Humphries, M. J., and Mould, A. P. (1994) *J. Biol. Chem.* 269, 4005–4011.
61. Chen, L. L., Lobb, R. R., Cuervo, J. H., Adams, S. P., and Pepinsky, R. B. (1998) *Biochemistry* 37, 8743–8753.
62. Chang, L. L., Truong, Q., Mumford, R. A., Egger, L. A., Kidambi, U., Lyons, K., McCauley, E. D., Van Riper, G., Vincent, S., Schmidt, J. A., MacCoss, M., and Hagmann, W. K. (2001) *Bioorg. Med. Chem. Lett.* 12, 159–163.
63. Bazzoni, G., Ma, L., Blue, M.-L., and Hemler, M. E. (1998) *J. Biol. Chem.* 273, 6670–6678.
64. Newham, P., Craig, S. E., Clark, K., Mould, A. P., and Humphries, M. J. (1998) *J. Immunol.* 160, 4508–4517.
65. Van der Vieren, M., Crowe, D. T., Hoekstra, D., Vazeux, R., Hoffman, P. A., Grayson, M. H., Bochner, B. S., Gallatin, W. M., and Staunton, D. E. (1999) *J. Immunol.* 163, 1984–1990.
66. Baneres, J. L., Roquet, F., Martin, A., and Parelo, J. (2000) *J. Biol. Chem.* 275, 5888–5903.
67. Yokosaki, Y., Matsuura, N., Sasaki, T., Murakami, I., Schneider, H., Higashiyama, S., Saitoh, Y., Yamakido, M., Taooka, Y., and Sheppard, D. (1999) *J. Biol. Chem.* 274, 36328–36334.
68. Smith, L. L., Cheung, H.-K., Ling, L. E., Chen, J., Sheppard, D., Pytela, R., and Giachelli, C. M. (1996) *J. Biol. Chem.* 271, 28485–28491.
69. Bayless, K. J., and Davis, G. E. (2001) *J. Biol. Chem.* 276, 13483–13489.
70. Teixeira, J., Parker, C. M., Kassner, P. D., and Hemler, M. E. (1992) *J. Biol. Chem.* 267, 1786–1791.
71. Parker, C. M., Pujades, C., Brenner, M. B., and Hemler, M. E. (1993) *J. Biol. Chem.* 268, 7028–7035.

BI020024D